Review

High Temperature Superconducting Flux Pumps for Contactless Energization

Zezhao Wen [1], Hongye Zhang [2,*] and Markus Mueller [1]

1 School of Engineering, University of Edinburgh, Edinburgh EH9 3JL, UK; zezhao.wen@ed.ac.uk (Z.W.); markus.mueller@ed.ac.uk (M.M.)
2 Department of Electrical and Electronic Engineering, University of Manchester, Manchester M1 3BB, UK
* Correspondence: hongye.zhang@manchester.ac.uk

Abstract: The development of superconducting technology has seen continuously increasing interest, especially in the area of clean power systems and electrification of transport with low CO_2 emission. Electric machines, as the major producer and consumer of the global electrical energy, have played a critical role in achieving zero carbon emission. The superior current carrying capacity of superconductors with zero DC loss opens the way to the next-generation electric machines characterized by much higher efficiency and power density compared to conventional machines. The persistent current mode is the optimal working condition for a superconducting magnet, and thus the energization of superconducting field windings has become a crucial challenge to be tackled, to which high temperature superconducting (HTS) flux pumps have been proposed as a promising solution. An HTS flux pump enables current injection into a closed superconducting coil wirelessly and provides continuous compensation to offset current decay, avoiding excessive cryogenic losses and sophisticated power electronics facilities. Despite many publications regarding the design and analyses of various types of HTS flux pumps, the practical application of HTS flux pumps in a high-performance superconducting machine has been rarely reported. Therefore, it is of significance to specify the main challenges for building and implementing a reliable HTS flux pump. In addition, the physical mechanisms of distinct HTS flux pumps have caused some confusion, which should be clarified. Above all, a systematic review of the recent development and progress of HTS flux pumps remains lacking. Given the above-mentioned issues, this paper summarized the most up-to-date advances of this emerging technology, clarified the working mechanisms and commonly adopted modeling approaches, presented objective analyses of the applicability of various HTS flux pumps, specified the primary challenges for implementing HTS flux pumps, and proposed useful suggestions to improve this wireless excitation technology. The overall aim of this work is to bring a deep insight into the understanding of HTS flux pumps and provide comprehensive guidance for their future research and applications.

Keywords: high temperature superconductor; flux pump; superconducting magnet; zero CO_2 emission; wireless energization

1. Introduction

The maturation of superconducting technology has led to a wide range of industrial applications and commercial products. Magnetic resonance imagining (MRI) and nuclear magnetic resonance (NMR) machines are vital equipment in modern medical diagnosis, which usually employ superconducting magnets to provide the required magnetic fields for physical examination of states of matter [1,2]. In the domain of motors/generators [3–10], superconductors have been attracting more and more attention since they are believed to be the optimal choice for electrification of large-size transport, such as electric aircraft, which requires the power density to be as high as possible. In the conceptual design of a hybrid-electric short-range aircraft A320 proposed by Rolls Royce and Siemens [11], a 10 MW,

7000 rpm superconducting generator employs high temperature superconducting (HTS) coils as the field winding and Litz wires for a two-layer distributed armature winding, which is capable of achieving a power density greater than 20 kW/kg. Another exemplary superconducting hybrid-aircraft project, funded by the German government, adapts the radial-flux-type fully superconducting electric motors and generators [12]. In this project, the rotor winding is composed of DC racetrack HTS coils and the stator winding consists of MgB_2 wires, both of which are cooled to 20–25 K by liquid hydrogen. It was estimated that these fully superconducting machines designs can achieve a power density no less than 38.1 kW/kg.

All the significant applications mentioned above rely on the superconductors to provide strong magnetic fields in an efficient way. It has been widely demonstrated that ultra-high magnetic fields can be obtained utilizing superconductors via various approaches [13–18]. Superconductor bulks have been fabricated to achieve a magnetic field of 17.24 T at 29 K using Y-Ba-Cu-O (YBCO) [19] and 17.6 T at 26 K [20], and [21] reported a trapped field of 17.7 T in a stack of superconductor tapes, all of which are an order of intensity stronger than a permanent magnet. However, the cost required for the corresponding cooling and charging system is extremely expensive and in some cases even unaffordable [22]. Advances made in the manufacture of coated conductors (CCs) [23–25], has enabled the production of long length superconducting CCs with robust bending tolerance suitable for winding superconductor coils. Compared to bulks and tape stacks, CC coils have much better mechanical properties [26] and flexibility in terms of demagnetization and ease of maintenance [27]. These benefits make superconducting CC coils a competitive candidate for high magnetic field usage, and thus lead to a critical question: how should superconducting coils be energized?

Technically, there are only two options for energizing a coil, namely direct injection and indirect induction. By the means of direct injection, coils are connected to a power supply and energized through current leads [28]. This straightforward approach can be excruciating when the current is especially high because the current leads for transmitting very high current are extraordinarily bulky, such as that in W7-X, where 17.6 kA is required [29]. Moreover, the multistage cooling used in a Large Hardon Collier (LHC) machine dictates the current while making the current leads more tortuous [30]. More importantly, the current leads physically bridge the cryostat with ambient environment at room temperatures, imposing heavy thermal loads for the cooling system [31–33] and resulting in substantial additional capital and operating costs [34]. This becomes a particularly severe problem for HTS coils, for which it is challenging to self-maintain a persistent current mode due to flux creep [35], so that the current leads need to be permanently placed during the operation. In order to tackle this problem, HTS flux pumps, which can constantly drive magnetic flux into a closed superconducting loop without physical connections, have been proposed, serving as an ideal alternative to direct injection.

The flux pump device, or flux pumping effect, was originally developed for low temperature superconductors (LTSCs) decades ago [36–46]. The fundamental principle can be summarized as: consider two superconducting loops connected, one of which acts as a flux driver to push flux into the other, once the flux arrives the receiving loop it can be constrained within the loop given that superconductors forbid flux either entering or escaping from them. The critical step is the creation of a locally normal region in a superconductor to form the switch, providing temporary passage for the flux. It was later discovered by Coombs et al. [47–49] that the elimination of superconductivity is not necessary for high temperature superconductors (HTSCs), leading to the new era of HTS flux pumps.

Since then, HTS flux pumps have been widely investigated over last decade. However, a systematic review that thoroughly summarizes the latest achievements is still not available [50–52]. Although HTS flux pumps were proposed for efficient energization, they also suffer from inherent losses by different means, depending on their specific configuration, which deserves more attention. The underlying physics of some HTS flux pumps

has been chronically debatable, which needs further clarification. This work reviews the roadmap and reports the latest state-of-art research progress, which is believed to provide a comprehensive overview for HTS flux pump technologies.

The rest of this article is structured as follows: Section 2 briefly introduces the early flux pumps for LTSCs and explains the factors that motivate the evolution to HTS flux pumps. Section 3 focuses on the travelling wave type flux pump, which is currently one of the most popular HTS flux pumps and provides detailed information for its underlying physics and modeling techniques. Section 4 describes the switched transformer-rectifier flux pump, as another important category of HTS flux pumps that has attracted increasing research interest. Section 5 also lists a set of other variants of HTS flux pumps, such as the thermally actuated, electronic-switch-based and pulse-type HTS flux pumps, whose working principles can be readily understood in the scope of those introduced in previous sections. All the existing HTS flux pump technologies are briefly summarized in Section 6. Section 7 elaborates the exploitation of HTS flux pumps in practical applications. On the basis of Sections 2–7, recommendations are proposed in Section 8 for the future development of HTS flux pump technologies.

2. Low Temperature Superconducting Flux Pump

Flux pump devices were firstly proposed based on LTSCs, by using a straightforward circuit theory. As described by Van de Klundert [53,54], the pumping procedure is illustrated in Figure 1. Travelling magnetic flux enters the L1 loop with switch S1 open and approaches closed switch S2; afterwards the switch S1 is closed while S2 is opened to let the flux transfer into the L2 loop. The flux is then contained within the L2 loop, and hence the load coil is magnetized. The whole process can be periodically repeated to accumulate flux and ramp magnetization for the load coil. Owing to this cumulative effect, a small magnetic field can result in a very high charging current in the load coil. Mulder et al. reported a thermally switched flux pump in 1991, capable of generating a current of 100 kA [55]. On the foundation of this principle, various flux pumps have been proposed, and details can be found in a dedicated review for early-stage flux pumps [53].
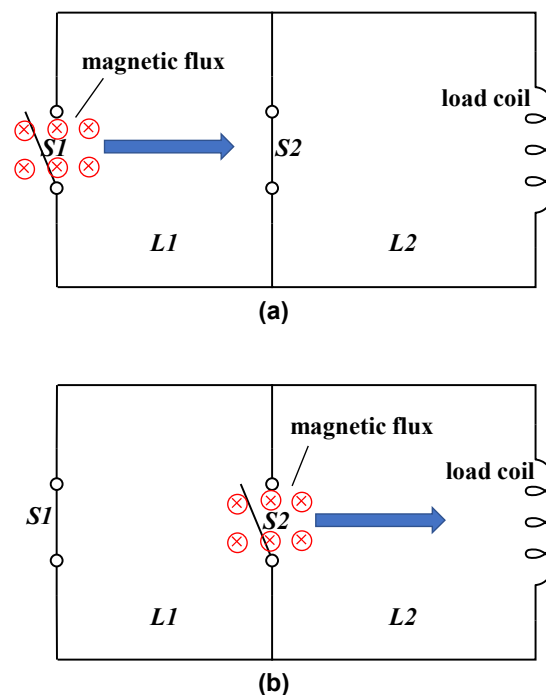
Figure 1. Illustration of flux pumping for LTSCs. Stage for (**a**) bringing flux into loop L1, (**b**) transferring flux into loop L2.

Initially, all flux pumps that take advantage of this flux pumping effect rely on a low temperature superconducting (LTS) switch to modulate the magnetic flux. To form an LTS switch in this type of flux pump, one can either choose the magnetic or thermal approach. For the magnetic approach, as shown in Figure 2, a magnetic field with its magnitude higher than the critical field H_c is applied to the LTS film to create a normal state region, which moves with the field synchronously. Alternatively, the magnetic field can be replaced by a heating source, which heats the area beneath beyond its critical temperature T_c, to create a normal state region. It is clear that either approach relies on the local elimination of superconductivity in the superconductors. However, the situation becomes quite different when it comes to HTSCs. Firstly, most HTSCs are type II superconductors, which have two critical fields H_{c1} and H_{c2} ($H_{c2} > H_{c1}$), where the upper critical field H_{c2} can be much higher than H_c of LTSCs. Therefore, it is hard to break the superconductivity of HTSCs by applying excessive magnetic fields. Similarly, driving HTSCs, which possess higher T_c, into normal state via overheating is also more difficult than that in LTSCs. It should be noted that thermal elimination of superconductivity for HTSCs is practically feasible, given that their transition temperatures are still much lower than the room temperature. Nevertheless, operating flux pumps with thermal activation, for each operation cycle, requires the HTS switch to be warmed up when the magnetic flux approaches and cooled down when the magnetic flux travels away, which severely restricts the operating frequency. In [56], Oomen et al. built a flux pump with HTS film, and heat was utilized to form the HTS switch, but the operating frequency was as low as 0.1 Hz. With such a low frequency, this kind of flux pump is not ideal for the majority of practical applications. Moreover, low frequencies can result in high ripples, as illustrated in [56] the flux ripple decreases by two orders of magnitude from 2400 to 60 ppm, when the operating frequency was increased to 50 Hz by replacing the HTS switches with MOSFETs.
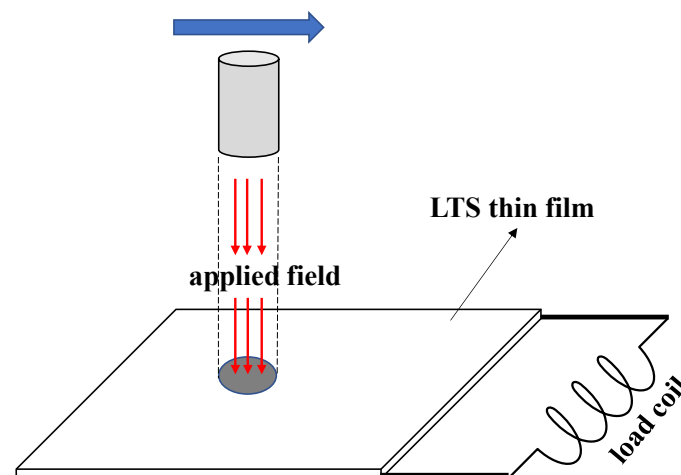
Figure 2. Illustration of magnetic switching for an LTS flux pump.

These above-mentioned issues have been considered critical obstacles for designing flux pumps with HTSCs. In 2007, Coombs et al. [47] built a test rig that successfully trapped a magnetic field of 0.2 T in a YBCO bulk. In their experiments, they used a thermal pulse to trigger a magnetic flux pulse travelling over the surface of an HTS sample, while the field was controlled by the change in magnetization or permeability. The significance of this experiment is that no normal regions have ever been created during the entire operation, implying that flux pumping can be achieved without breaking superconductivity for HTSCs. Following this novel discovery, tremendous efforts have been made by worldwide research groups to deeply investigate this phenomenon, leading to remarkable advancements for HTS flux pumps.

3. Travelling Wave HTS Flux Pumps

Inspired by the experimental tests in [47], it has been widely demonstrated that HTS flux pumps can be achieved by employing travelling magnetic waves. The generalized schematic diagram for a travelling wave HTS flux pump is illustrated in Figure 3a, which can be modeled by the equivalent circuit in Figure 3b. When an alternating magnetic field travels across the surface of HTSCs (typically HTS tapes), eddy currents will be induced and circulated within the superconductor. The current then results in an electric field, whose time-averaged integration over one cycle is derived to be a non-zero value. If the HTS tapes are connected to a load (usually HTS coils) to from a closed loop, then the flux pump can be considered as a DC voltage source V_{oc}, with internal resistance of R_V, charging an inductive load that has an inductance of L and resistance of R_L through resistive joints R_J. The whole system can be described by a Kirchhoff voltage equation:
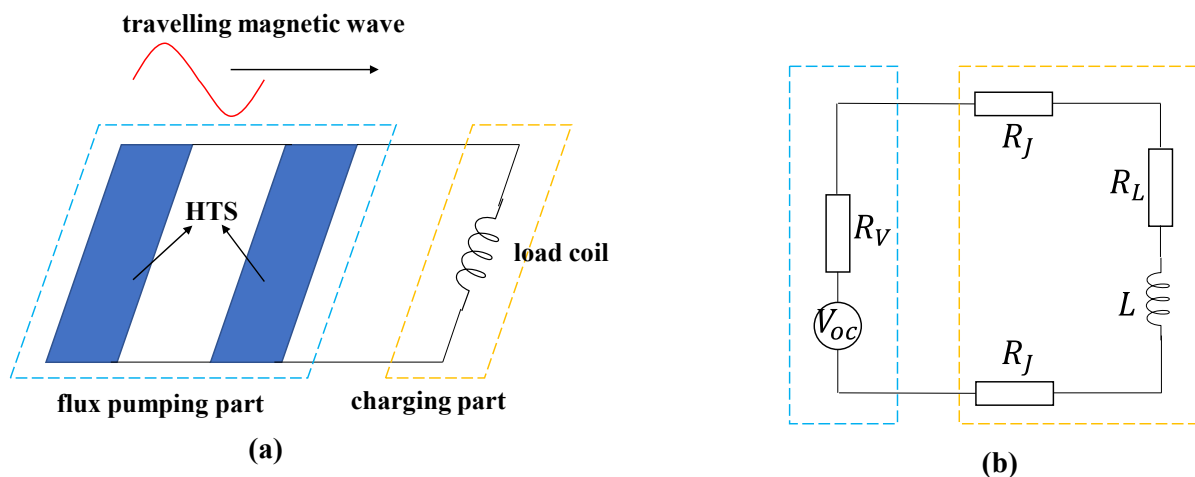
$$V_{oc} = I(R_V + 2R_J + R_L) + L\frac{dI}{dt} \tag{1}$$

Under zero-state response, the pumped current I can be calculated as:

$$I = I_s\left(1 - e^{-(\frac{1}{\tau})t}\right) \tag{2}$$

where I_s is the steady state current, i.e., the maximum pumped current, τ is the time constant that is determined using the following equation:

$$\tau = \frac{L}{R_V + 2R_J + R_L} \tag{3}$$

Figure 3. (**a**) Schematic diagram, (**b**) equivalent circuit for travelling wave HTS flux pump.

The most important step in operating a travelling wave HTS flux pump is to provide proper alternating magnetic fields, for which effective DC voltage can be induced. According to the ways in which the magnetic fields are provided, travelling wave flux pumps can be classified to rotary HTS flux pumps and linear HTS flux pumps.

3.1. Rotary HTS Flux Pumps

HTS rotary flux pumps, or so-called HTS dynamos, firstly proposed by Hoffman et al. [57], employ one or multiple permanent magnets (PMs) mounted on a rotating disc as shown in Figure 4. The rotation of disc causes spatially varying magnetic fields and forms the travelling wave required by the flux pumps.
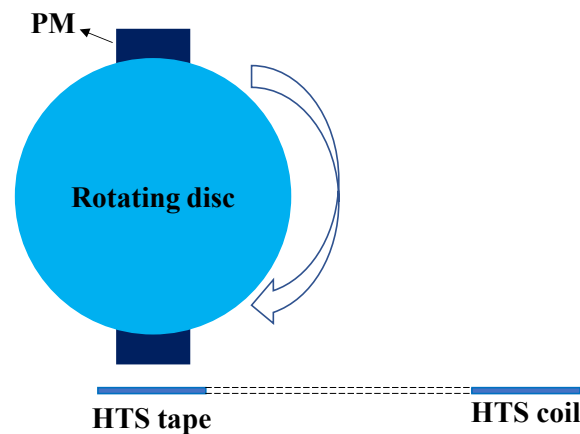
Figure 4. Cross section view of a rotary HTS flux pump equipped with two PMs.

This type of HTS flux pump has been extensively investigated, because of its simple structure and ease of operation. The basic design considerations for an HTS dynamo are the generated voltage and pumped current [58]. From Equation (1), the pumped current is directly determined by the effective DC voltage induced in the HTS tapes. Abundant work has been conducted to characterize the open circuit voltage for HTS dynamos, mainly credited to the research groups of the Robinson Research Institute, Victoria University of Wellington [59–62]. Inspired by the basic configuration of HTS dynamo, experiments were performed to investigate the impact of the flux gap [63], frequency (disc rotating speed) [64], tape width [65], and geometry of magnets [66] upon the open circuit voltage V_{oc}. Generally, it has been demonstrated that V_{oc} increases with the frequency and tape width but decreases with the flux gap. In terms of the magnet geometry, it was concluded in [66] that the generated voltage is insensitive to the orientation of the magnet but can be influenced by the magnet cross-section area. More precisely, the generated voltage shows a linear rise versus the frequency until a turning point usually appears around hundreds of Hz. After this turning frequency, nonlinear variation in the output voltage occurs, i.e., the slope of the voltage–frequency curve begins to decrease with frequency. This experimental observation was rather overlooked and not well explained until Zhang et al. [67,68] proposed and demonstrated the use of a multilayer model to investigate the electromagnetic losses in HTS-coated conductors over a wide range of frequencies. It was found in [67,68] that at frequencies higher than 100 Hz in the case of magnetization, the skin effect plays a dominant role in the determination of current distribution in an HTS CC, which results in the current drifting from the HTS layer to other non-superconducting layers, e.g., the copper stabilizers. Hence, the electric field established by the superconducting current is weakened, and thus the generated voltage experiences a progressive decrease with increasing frequencies. It is worthwhile mentioning that this is also the reason for which numerical models that only consider the HTS layer cannot manifest the nonlinear frequency response but predict a constant linear rate of increase in voltage. The generated voltage is consistently inversely proportional to the flux gap because the magnetic field experienced by the HTS tape is inversely proportional to the flux gap.

In contrast to the monotonic relationships described above, the generated voltage varies parabolically with HTS tape width in [69], namely the voltage initially increases up to a certain point and then starts to decrease as the tape width increases, which means there exists an optimal value for the tape width in order to achieve the highest voltage. However, it was found in [70] that the voltage will saturate at a certain point, after which further increase in the tape width has little impact on the voltage. The different relationships are attributed to whether or not a constant flux gap is maintained when the magnet passes over the HTS tape. The HTS dynamo modeled in [69] adopts the radial flux geometry, where the HTS tape and PM surface are flat so that the distance (along the magnetization direction) between the magnet and the tape varies as the magnet rotates, as shown in

Figure 5a. As a comparison, the model in [70] still adopts the radial flux geometry but the surface of magnet and HTS tape are curved, which will result in a constant air gap (along the magnetization direction) between the magnet and HTS tape, as shown in Figure 5b. The underlying physics causing this peculiar bilateral tape width effect have not been reported yet, which requires further investigation. Regarding the configuration of HTS dynamos, it should be noted that a constant flux gap can also be achieved by adopting the axial flux geometry, in which the magnet is rotating in a plane parallel to the HTS tape surface, as shown in Figure 5c.
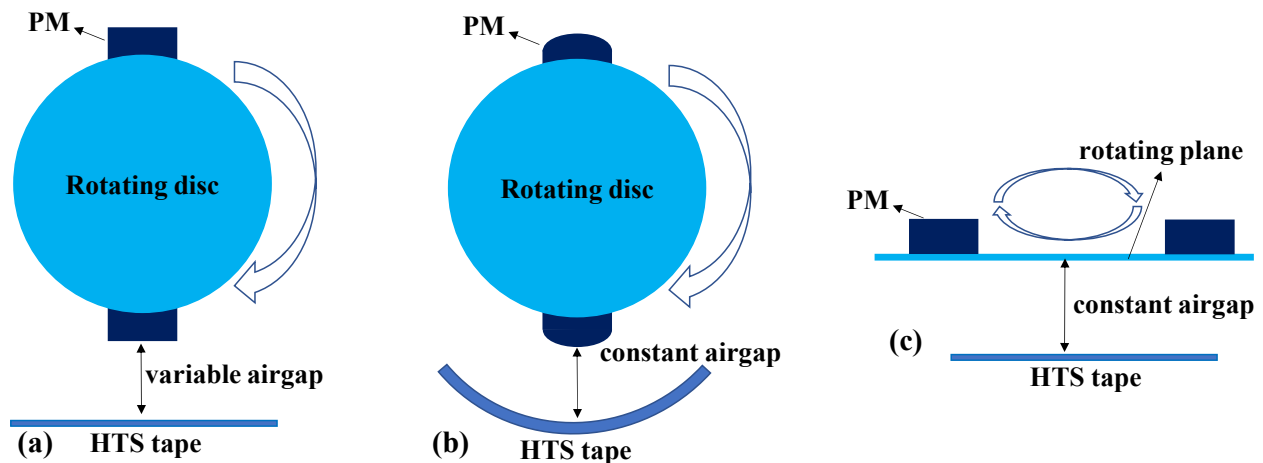

Figure 5. Cross section diagram for different HTS dynamo configurations: (**a**) axial flux geometry with non-uniform airgap, (**b**) axial flux geometry with uniform geometry, (**c**) radial flux geometry with uniform airgap (the rotating plane is perpendicular to the paper).

3.2. Linear HTS Flux Pumps

A travelling wave HTS flux pump utilizes static electromagnets rather than rotating PMs to provide the alternating magnetic fields required for generating effective DC voltage in HTS tapes. The whole device resembles the structure of a linear motor and is named as a linear HTS flux pump.

This type of HTS flux pumps has been mostly explored by the HTS group at the University of Cambridge [71–74]. Figure 6 shows a typical structure of an HTS linear flux pump. This flux pump consists of eight copper coils in four columns, in each column an HTS tape is sandwiched by an upper and lower copper coil connected in series. Each copper coil is wound around laminated iron cores and supported by an iron framework to focus the magnetic flux. The four HTS tapes are connected in parallel across the HTS coil.
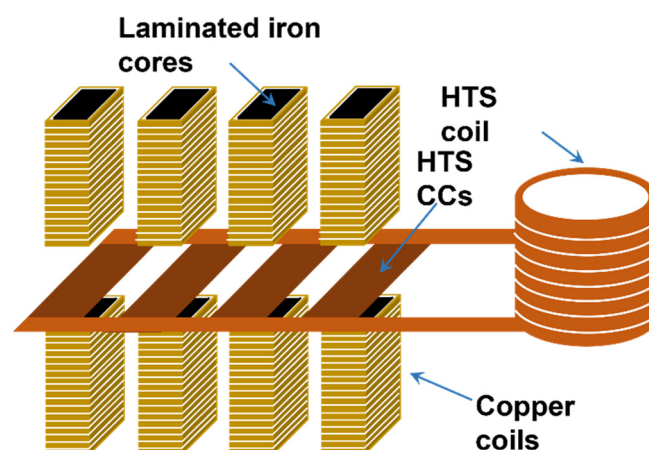

Figure 6. Schematic diagram for a linear HTS flux pump.

The linear HTS flux pump is operated by successively exciting each set of copper coils, forming a modulated field fluctuation in space that is analogue to a travelling wave. Experiments have demonstrated [72] that the pumping performance can be influenced by the frequency, amplitude, and waveform shape of the excitation current. Basically, the flux pumping is an accumulation process, where the current in the load coils is subsequently pumped up in each operation cycle. The limits are principally determined by the critical current I_c of the HTS tape rather than the magnetic field. Linear HTS flux pumps were observed to pump more or less the same current when operated at different frequencies and amplitudes, although a higher frequency and/or amplitude resulted in faster charging. For the waveform profiles, a triangular wave was demonstrated to be more effective than trapezoidal and sinusoidal waves. The authors of [71] found that a standing waveform, e.g., by exciting only one of the copper coils, can also energize the HTS load coils, which was thought to be an anomalous exception, as no travelling waves are present. In fact, this phenomenon can be explained if one considers the origin of the voltage generation in the HTS tapes, which will be clarified in detail in the following subsections.

3.3. Underlying Physics

The travelling wave flux pump is a phenomenological subject, for which the underlying physics have been mysterious for years. Consider the flux pumping part in Figure 3a, it is topologically identical to an AC alternator, where only AC voltage is supposed to be induced under AC fields without DC components. In 2014 [75], seven years later after the discovery of HTS flux pumping effects under travelling wave, Coombs et al. firstly gave a clue that the crucial difference between HTS travelling wave flux pumps and conventional AC alternators is likely to relate to the non-linear *E-J* characteristics, though no exhaustive explanation was given then. The first dedicated work that attempts to clarify the origin of the voltage observed in an HTS travelling wave flux pump was published by Geng et al. in 2016 [76]. They developed theoretical analysis based on a simple circuit, as shown in Figure 7, that is intuitively identical to the arrangement of a linear HTS flux pump shown in Figure 6, where superconducting loops can be formed by two adjacent HTS tapes.
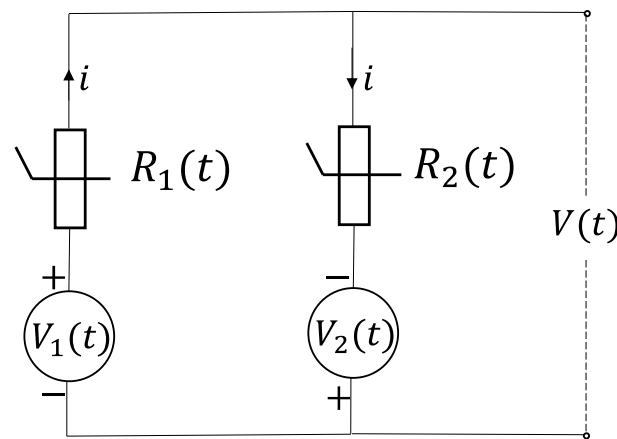
Figure 7. Electric circuit for analyzing the voltage generation.

The open circuit voltage across the HTS loop is:

$$V(t) = iR_2(t) - V_2(t) = \frac{V_1(t) + V_2(t)}{R_1(t) + R_2(t)} R_2(t) - V_2(t) \tag{4}$$

Taking the time average derives the effective DC voltage as:

$$V_{dc} = \frac{1}{T} \int_0^T V(t) dt = \frac{1}{T} \int_0^T \frac{-d\Phi/dt}{R_1(t) + R_2(t)} R_2(t) dt \tag{5}$$

where $V_1(t)$ and $V_2(t)$ represent the electromotive force induced in each HTS tape, while $R_1(t)$ and $R_2(t)$ represent their resistance accordingly. T is the cycle period of the applied field and Φ is the total flux applied to the HTS loop. To fulfill the Faraday's law, $\int_0^T V_2(t)dt$ is zero. If the resistance in each HTS tape is constant throughout the operation, i.e., $\frac{R_2(t)}{R_1(t)+R_2(t)}$ equals a fixed value, the effective voltage must be zero. However, if the resistances are time varying functions, it is possible that Equation (5) can lead to a finite non-zero result, which shapes the effective DC voltage. Geng et al. then discussed the field strength, the influence of rate of field change on the resistance, and hence attributed the DC voltage to the variation in the resistivity of type II superconductors.

Almost at the same time, in 2016, Bumby et al. [77] published an enlightening work to explain the DC voltage origin for an HTS dynamo. In their work, the Giaver model was applied, which considers that the superconducting eddy currents "short-circuit" the high field region, e.g., the region beneath the PM during the passage of PM across the HTS tape as shown in Figure 8a,b. Under this assumption, the circulating current is expected to spread over the tape, such that:

$$\delta(\theta)J_{ser} = -(w - \delta(\theta))J_{sh} \tag{6}$$

where J_{ser} is the induced average local current density in a region of the HTS tape that is directly beneath the magnet, $\delta(\theta)$ is the path width at rotor angle θ, and J_{sh} is the concomitant returning current. The flux–flow resistance in type II superconductors can be described by **E-J** power law:

$$\boldsymbol{E} = E_c \frac{\boldsymbol{J}}{J_c}\left(\frac{|\boldsymbol{J}|}{J_c}\right)^{n-1} \tag{7}$$
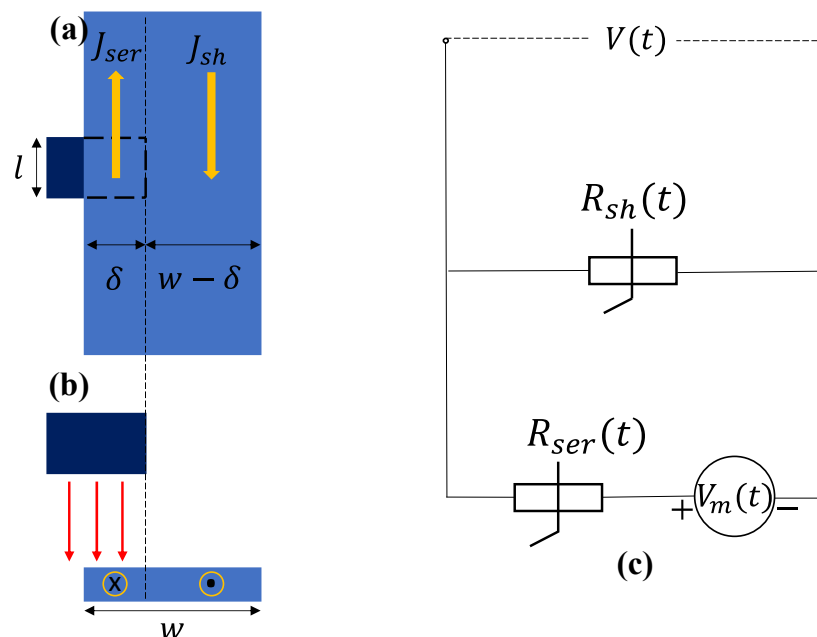
Figure 8. Schematic diagram illustrating the circulating current as the magnet rotates over the HTS tape (**a**) vertical view, (**b**) front view, (**c**) circuit sketch.

Hence, the resistances in each of the circulating paths can be expressed as:

$$R = \frac{lE_0|\boldsymbol{J}|^{n-1}}{(w-\delta)J_c{}^n} \tag{8}$$

Consider the analysis of the circuit in Figure 8c, the instantaneous representation of that effective DC voltage can be derived as:

$$V(t) = \frac{-V_m(\theta)}{1 + \left(\dfrac{\delta(\theta)}{w - \delta(\theta)}\right)^n} \tag{9}$$

where J_c is the critical current density at a threshold field E_c, n is a constant coefficient related to the materials. V_m is approximated as $V_m = lvB$, with l and v representing the length and linear velocity of the magnet and B is the flux density, for the magnet passing over the tapes. Otherwise, it is always zero. This equation was able to show qualitative agreement with the experimental measurements, implying that the circulation of superconducting current seems to be the cause of the DC output voltage from an HTS dynamo. Following this work, Mataira et al. further demonstrated in [78] that the circulating superconducting current under the strong field region substantially exceeds the local critical current density and triggers a highly non-linear resistivity, leading to bizarre distortions on the induced AC waveform. As a result, the net integration of the AC waveform is no longer zero and forms an effective DC component. The same group then clearly stated that it is the non-linear resistivity and unsymmetric eddy current effect that gives rise to the DC output voltage from an HTS dynamo [79]. Thanks to that, the longstanding conundrum should have now been clarified clearly.

As an alternative to the microscopic approach presented above, Wang et al. proposed a macroscopic theory [80] to explain the DC voltage generation in an HTS travelling wave flux pump. According to their explanation, the local-field inhomogeneity, i.e., a DC biased AC waveform, causes a coupling effect between clusters of coupled vortices and the applied magnetic poles, and the coupling force drags the vortex cluster into the HTS film and hence traps flux within it, as illustrated in Figure 9. The physics conceived in [80] tends to oppugn the non-linear resistivity established in [78,79], as they stated in [81]. The focus of the debate is that a pure AC waveform cannot prompt a DC output from a travelling wave flux pump, which was not clearly studied in [78,79]. However, the zero DC output voltage in a travelling wave HTS flux pump under pure AC fields should not be taken as evidence that challenges the theory based on the non-linear resistivity.
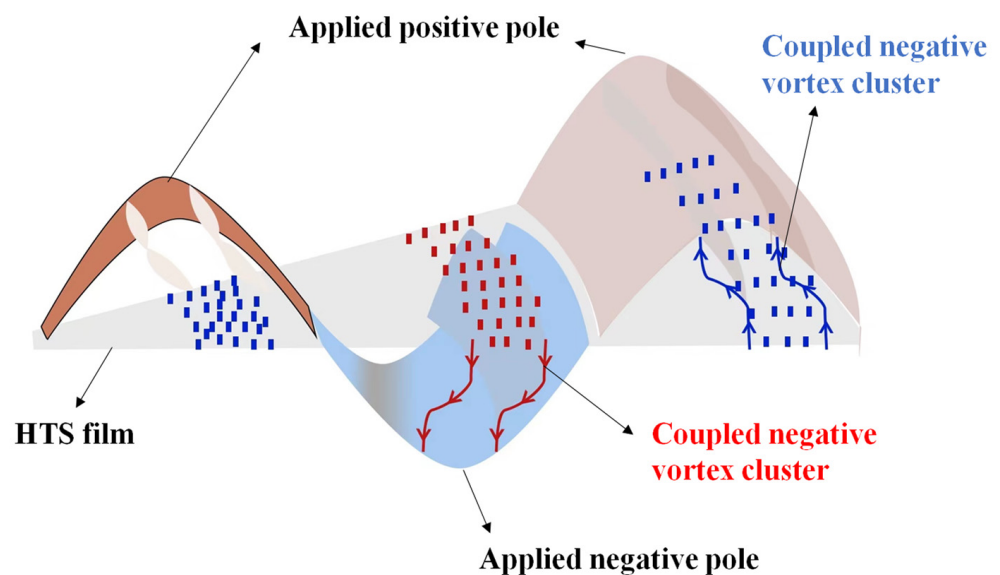
Figure 9. Coupling features including the ramping up of vortex density and misalignment between applied pole and coupled cluster. Adapted from [80].

Based on Equation (7), one can describe the net averaged DC voltage as:

$$V_{dc} = \frac{E_c}{J_c{}^n} \frac{1}{S} \frac{1}{T} l \int_0^T dt \oiint J|J|^{n-1} ds \qquad (10)$$

For an open circuit, there must be no transport current such that:

$$\oiint J ds = 0 \qquad (11)$$

Thus, V_{dc} must be zero if $n = 1$, similar to that in a normal conductor. For $n > 1$, such as that in a superconductor with non-linear resistivity, J is spatially dependent and it can lead to a finite non-zero solution for Equation (10). Alternatively, one can also express the net averaged DC voltage directly from the Faraday's law:

$$V_{dc} = \frac{1}{T} \int_0^T dt \oiint \frac{dB(x,y,t)}{dt} ds = \oiint \frac{1}{T} [B(x,y,t=T) - B(x,y,t=0)] ds \qquad (12)$$

If the applied magnetic field $B(x,y,t)$ is a pure AC waveform, then at any position it must hold that $B(x,y,t=T) = B(x,y,t=0)$, so V_{dc} can only be zero. Equations (10) and (12) can both hold simultaneously and agree well mathematically with each other. The physical interpretation is simply that if the applied field is pure AC and hence completely identical in the positive and negative cycles, the waveform distortion (of course still originates from the non-linear resistivity) is cancelled out during the whole periodic operation. Thus, applying a pure AC field should be considered as a special scenario instead of a counterexample of the theory built on non-linear resistivity.

3.4. Modeling Techniques

Various formulations have been successfully implemented into commercial software, e.g., COMSOL Multiphysics, for HTS flux pump modeling. Generally, the electromagnetic behaviors involved in operating a travelling wave HTS flux pump can be well described by Maxwell equations. Depending on the state variables selected for solving Maxwell equations, different formulations can be utilized, such as the H formulation [82–86], coupled H-A formulation [87,88], and coupled T-A formulation [89–93]. In addition, extra techniques have been developed to simplify the solution of Maxwell equations in specific aspects, including the H-formulation with shell current [70,78,79], segregated H-formulation [94,95], minimum electromagnetic entropy production (MEMEP) [96,97], integral equation (IE) [98–100], volume integral equation-based equivalent circuit (VIE) [101–103], and Chebyshev polynomials based methods [104–106]. Exhaustive details for each formulation can be found in the benchmark paper [107] published by Ainslie et al., which is strongly recommended to readers for acquiring information about HTS dynamo modeling. In addition, two remarks should be supplemented. The first one is, all models in [107] follow a classical assumption that the critical current of the HTS tape is constant. However, the critical current is sensitive to the magnetic field experienced by the HTS tapes, which has been shown to have significant impacts on the generated voltage [78]. Fortunately, in terms of numerical modeling, one can easily include this feature by importing the experimentally measured critical current under different fields to the model. Alternatively, one can describe the field dependence of critical current by an empirical function:

$$J_c(B) = \frac{J_{c0}}{\left(1 + \frac{\sqrt{k^2 B_{para}{}^2 + B_{perp}{}^2}}{B_0}\right)^\alpha} \qquad (13)$$

where B_{para} and B_{perp} represent the parallel and perpendicular components of the magnetic flux density with respect to the wide face of superconducting tape. J_{c0}, B_0, k, and α are

constant coefficients related to materials. It also should be pointed out that the models in [107] only consider the superconducting layer of an HTS tape. This approximation is valid only under low frequencies, because for relative higher frequencies (hundreds of Hz or above) the currents induced by external magnetic fields tend to be drawn away from the HTS layer to its edges due to the skin effect, which cannot be reflected by a single layer model [108]. Therefore, it is necessary to consider all layers in a coated HTS conductor, e.g., the copper stabilizers, silver overlayer as well as substrate. With the two remarks added, one should obtain a numerical model that possess the full capability to simulate the behavior of a travelling wave HTS flux pump. Up to now, most of the modeling techniques are mainly implemented for a rotary HTS flux pump, due to its structural simplicity. As discussed in Section 3.3, the rotary HTS flux pump and linear HTS flux pump share exactly the same physical mechanism. The modeling techniques for HTS dynamos modeling can be confidently transferred to model HTS flux pumps, while the only difference lies in modeling the applied field either by a remanent flux density (for PMs) or an excitation current (for electromagnets). The general framework for modeling an HTS dynamo can be illustrated as that in Figure 10.
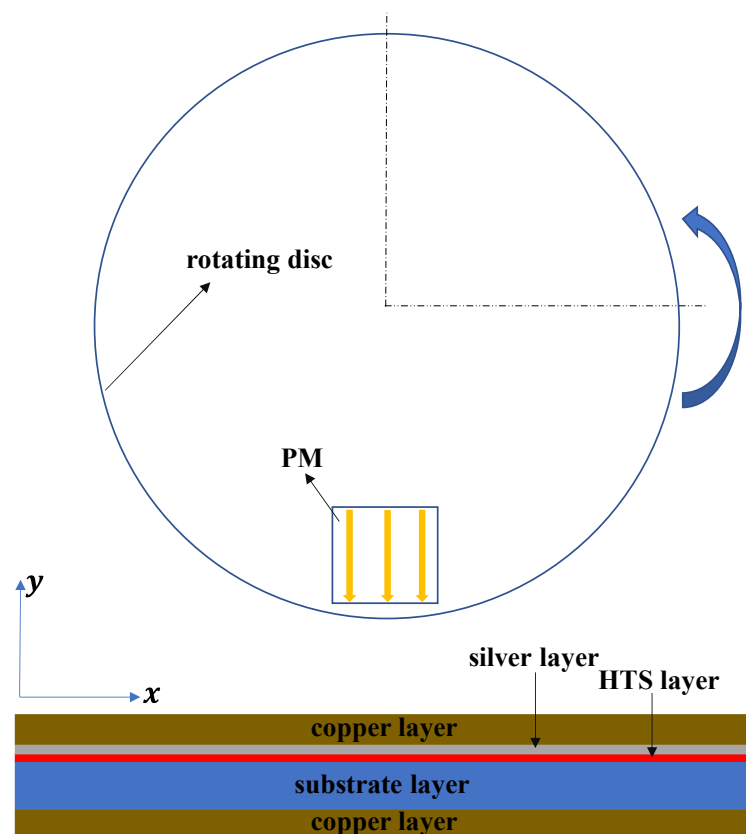
Figure 10. Illustration of the modeling framework for an HTS dynamo (cross section view), and the golden arrows identify the polarization of PM, the blue twisted arrow means the rotating direction of the disc.

In addition to the widely used 2D models, Asef et al. [109] proposed the first 3D model for an HTS dynamo, based on the MEMEP approach that they initially proposed for 2D HTS dynamo modeling. This model has shown good agreement with experiments as well as the 2D models. The highlight of this model is that it visualizes the screening current and electric field distribution across the HTS tape surface, which is significant as it provides evidence for the mechanism explanation based on the eddy current circulation. So far, the models discussed above usually only cover the flux pumping part shown in Figure 3a, aiming to investigate the open circuit voltage output. In order to replicate a travelling wave

HTS flux pump in full, one should also include the superconducting coils under charge. The authors of [110] modeled the full charging process for an HTS dynamo, where the load coils are simplified as a series combination of an inductor and resistor with predetermined values. To link the flux pumping part with the load coils being charged, the constraint imposed to maintain the current in HTS tapes, as previously described by Equation (11), should be amended accordingly:

$$\oiint J ds = I_t \tag{14}$$

where I_t denotes the currents stimulated (by the induced voltage across the HTS tapes) in the coils and hence also flowing through the HTS tapes as a complete circuit loop.

4. Transformer-Rectifier HTS Flux Pumps

HTS flux pumps can be achieved in the magnetic field driven mode, as detailed in Section 3, while they can also be realized in the current driven mode, which are classified as transformer-rectifier HTS flux pumps. A general schematic drawing is shown in Figure 11. An alternating current i_1 is induced in the secondary winding of the transformer, which is connected to the HTS bridge and coil and forms two loops in parallel. Initially, the HTS bridge short-circuits the HTS coil, and i_2 flows through loop1 only (i.e., $i_1 = i_2$). Under certain conditions, the HTS bridge can exhibit temporary resistivity; thus, breaks the short circuit and forms a rectifier. Consequently, the HTS coil can be charged by a current i_L flowing in loop2. When the HTS bridge eliminates its resistivity, the HTS coil is again short-circuited and hence flux is trapped. The flux pumping process involved here is, in essence, similar to LTS flux pumps. The difference is that the resistive region in HTSCs (analogue to the normal region in LTSCs) requires no elimination of superconductivity. Depending on how to trigger the resistivity in the HTS bridge, there are AC field switched [111–114] and self-regulating transformer-rectifier HTS flux pumps [115–117].
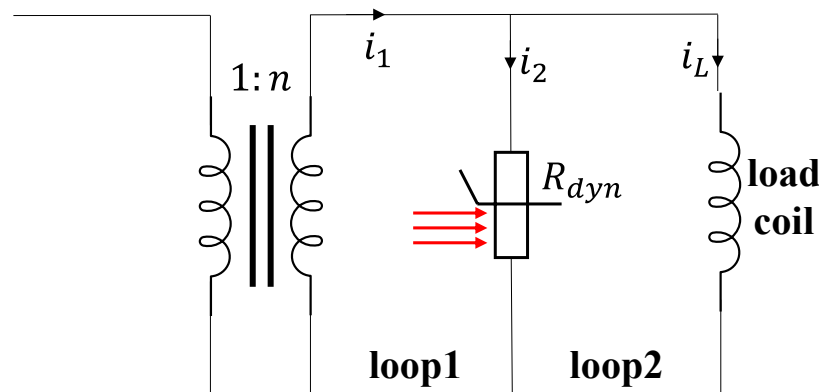
Figure 11. Circuit diagram for a transformer-rectifier HTS flux pump (red arrows denote the applied magnetic field).

4.1. AC Field Switched Transformer-Rectifier HTS Flux Pumps

4.1.1. Topology

This type of flux pump, as shown in Figure 12, was firstly demonstrated by Geng and Coombs [112]. When the HTS bridge carries a current i_2 induced in the secondary winding, an alternating magnetic field is applied perpendicularly to the surface of the HTS bridge. As long as i_2 flows in one direction in the HTS bridge with the existence of the alternating field, resistivity can be triggered.
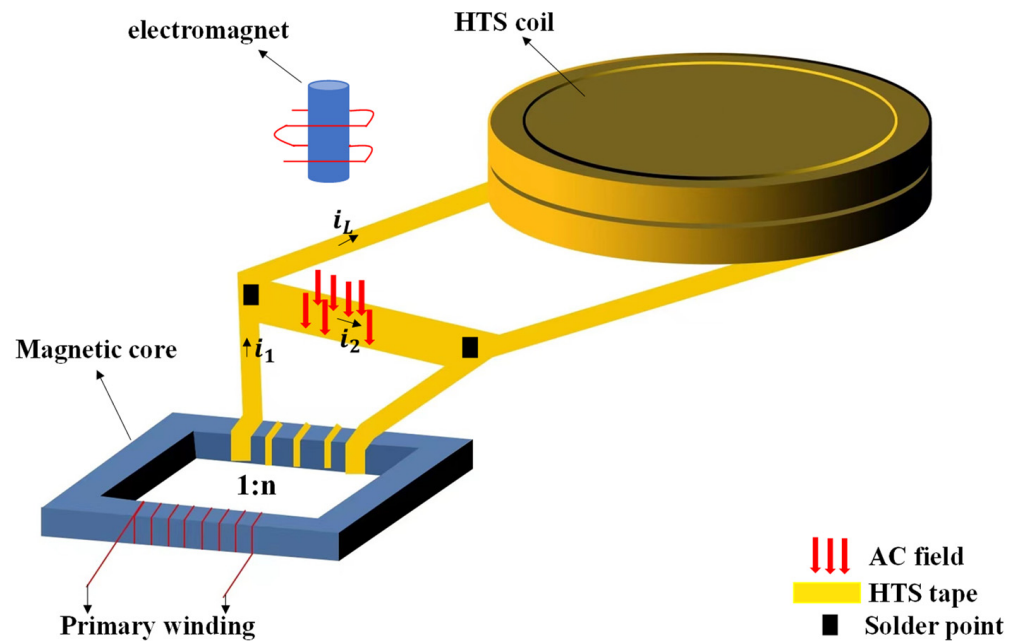
Figure 12. Structure diagram of an AC field switched transformer-rectifier HTS flux pump.

Several influential factors on the flux pumping performance were examined in the comprehensive research presented in [111], including excitation current magnitude, applied field magnitude, frequency and duration, and phase differences between current and field. Briefly, the pumping current decreases from its maximum at no phase misalignment (the transporting current is in phase with the field) to zero at 90 degrees phase difference; an increase in either the strength or frequency of the applied field leads to a continuously increasing pumped current; the duration of the applied field (i.e., how long the resistivity in the HTS bridge is maintained) has negligible impact on the pumping current. The influence of the excitation current is relatively more complicated: the pumping current increases with the excitation current magnitude up to a turning point, after which it starts to drop if the excitation current increases further, implying that there exists an optimal excitation current to maximize the pumping current. In addition, it was found in [118] that adding an actual resistance to the secondary winding can enhance the pumping current, especially when the desired current is high.

4.1.2. Mechanism

The working principle of an AC field switched transformer-rectifier HTS flux pump is crystal clear, since it is completely based on the well described dynamic resistance effect [119–121]. It is known that the external magnetic field B_{ext} penetrates certain distance into the superconductor from its edges. The penetration depth increases with the magnetic field. Hence, if the magnetic field is strong enough, it can penetrate the central area and create a resistive region as shown in Figure 13.

Under such conditions, the current flows in the central area tends to interact with the magnetic flux and cannot flow without resistivity. The widely accepted formula to calculate dynamic resistance R_{dyn} was proposed in [121], which can be expressed as:

$$R_{dyn} = \frac{2wlf}{I_c}(B_{ext} - B_{th}) \tag{15}$$
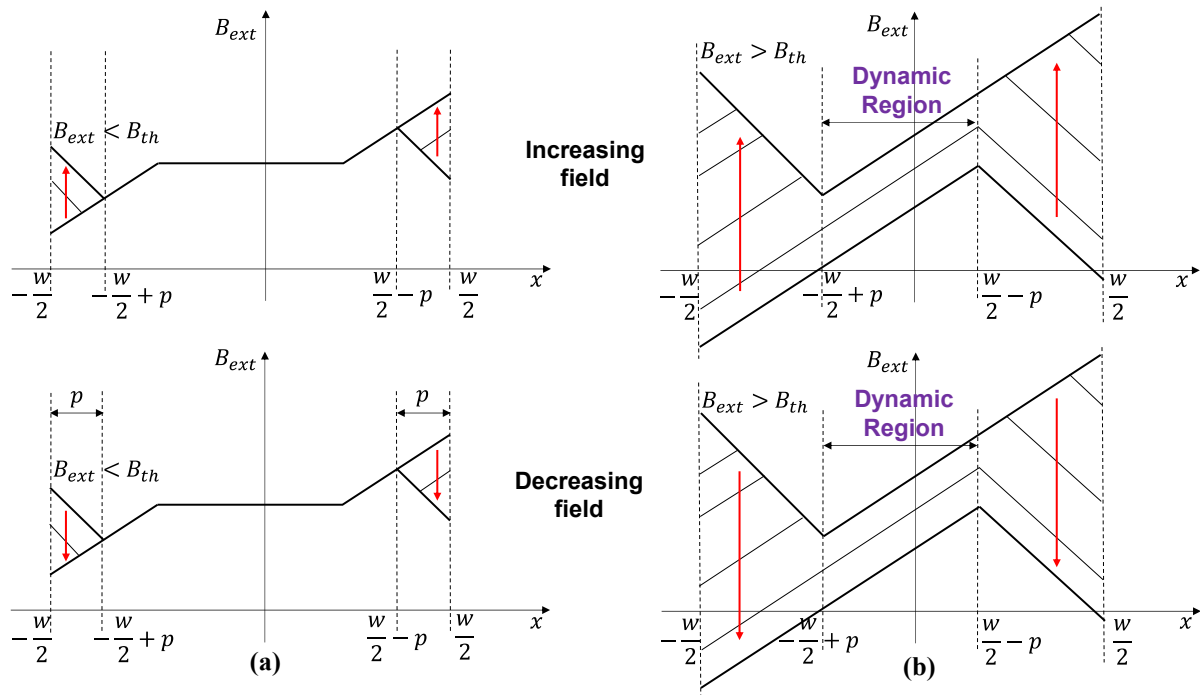
Figure 13. Magnetic profile inside an HTS conductor when it carries a DC current under an AC magnetic field. (**a**) The applied field B_{ext} is smaller than the threshold B_{th}, (**b**) the applied field B_{ext} exceeds the threshold B_{th} and creates the dynamic region. Adapted from [121].

However, this linear formula cannot reflect the non-linearity of dynamic resistance. Equation (15) was then complemented by Zhang et al., in [120], where a second term was added to account for the non-linear contribution:

$$R_{dyn} = \frac{2wlf}{I_c}(B_{ext} - B_{th}) + \frac{E_c l}{I_t} i^{n+1} f_{avg}(B) \tag{16}$$

$$f_{avg}(B) = 1 + \sum_{p=0}^{\frac{n}{2}-1} \left\{ \frac{n!}{(2p+1)![n-(2p+1)]!} \left(\frac{B_{ext}}{B_0}\right)^{2p+1} \frac{2^{p+1} \cdot p!}{\pi \prod_{q=0}^{2p+1}(2q+1)} + \frac{n!}{(2p+2)![n-(2p+2)]!} \left(\frac{B_{ext}}{2B_0}\right)^{2p+2} \frac{(2p+2)!}{[(p+1)!]^2} \right\} \tag{17}$$

where w is the width of the superconductor, l is the length of superconductor subjected to the field, I_c is the critical current, B_{ext} and f are the amplitude and frequency of the applied field, respectively. B_{th} represents the threshold that the applied field must exceed to create the dynamic region. i is the load ratio that reflects proportions of transport current I_t to the critical current, i.e., $I_t = iI_c$. n in Equation (17) is even and in the case of an odd n, the formula has to be adapted accordingly as illustrated in [120]. It should be noted that Equation (15) was initially developed for a superconductor carrying DC current, but the HTS bridge transports an alternating current. It is still applicable here because the field is only applied when the current flows in one direction.

4.2. Self-Regulating Transformer-Rectifier HTS Flux Pumps
4.2.1. Topology

Following the design in Figure 12, Geng et al. [122] further developed the self-regulating transformer-rectifier HTS flux pump, which are hand-in-hand with the AC field switched ones. The two prototypes share almost the same topology, whilst the only difference is whether the field generating component is included. In a self-regulating transformer-rectifier HTS flux pump, the AC magnetic field is no longer required to trigger resistivity in the HTS bridge. Alternatively, a highly asymmetric (the absolute value of positive peak is much higher than its negative peak) current is injected into the primary

winding. Then, resistivity can be trigged for the HTS bridge when it conducts the positive peak current. With this approach, it eliminates the troublesome field modulation, making the whole operation solely driven by current. As a result, the operational considerations are less than that for an AC field switched HTS flux pump, principally only the magnitude and frequency of the primary current. As experimentally demonstrated in [122], unlike the AC field switched ones, where the primary current magnitude has a bilateral effect, the pumping current for a self-regulating flux pump continuously increases with the primary current. More or less the same pumping current was obtained for various primary current frequencies, but faster charging speed was observed under higher frequencies.

4.2.2. Mechanism

Intuitively, due to the topological similarity, the mechanism of self-regulating flux pumps is close to the AC field switched ones, but slightly different. For type II superconductors, the current and electric field relations normally can be described by the exponential **E-J** power law as Equation (7). Visualizing this equation, as shown in Figure 14, one can find that if the current density exceeds a threshold value, the superconductor will enter the flux flow regime and exhibit obvious resistivity. Thus, if some parts of the secondary current waveform (e.g., the positive peak region) are greater while all the rest are smaller than the threshold, the HTS bridge can possess temporary resistivity in one cycle and hence provides the rectification effect. This is the reason why the primary current must be highly asymmetric, and the flux pump can only operate in half-wave mode.
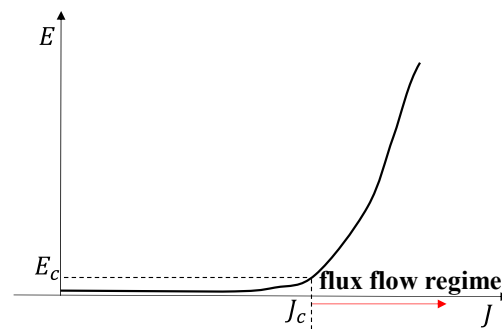
Figure 14. Visualization of the **E-J** relation, the red arrow means that the flux flow regime appears after transport current exceeds the critical current density.

4.3. Modeling Techniques

Theoretically, the methods detailed in Section 3.4 for travelling wave HTS flux pumps modeling are applicable to the above two types of HTS flux pumps. Most previous work about transformer-rectifier HTS flux pumps are experimental, a good example of the modeling can be found in [123]. Based on the circuit diagram in Figure 11, the transformer can be equivalently substituted by a magnetic field applied perpendicularly to loop1, which can induce a circulating screen current, accordingly. The whole system then can be simplified to three parallel HTS tapes (S_1, S_2 and S_L) connected at the terminals, which is reflected by a global constraint equation:

$$i_{S_1} + i_{S_2} + i_{S_L} = \oiint J_{S_1} ds + \oiint J_{S_2} ds + \oiint J_{S_L} ds = 0 \tag{18}$$

Later, a novel modeling approach was proposed in [124]. Different from those formulation-based models aiming to solve Maxwell equations, this model completely relies on the circuit analysis for Figure 11. By combining Equations (7) and (15), one can express the net output voltage across the HTS bridge as:

$$V_{out} = i_2 \frac{2wlf}{I_c}(B_{ext} - B_{th}) + E_c l \frac{i_2^{\,n-1}}{I_c^{\,n}} \tag{19}$$

which can then be utilized to calculate the current in an inductive coil with fixed inductance, similar to Equation (1). This method evades sophisticated electromagnetic interactions that occur in the real operation by applying a set of approximated equations, so it is much more efficient than finite element methods (FEM), in terms of solution time.
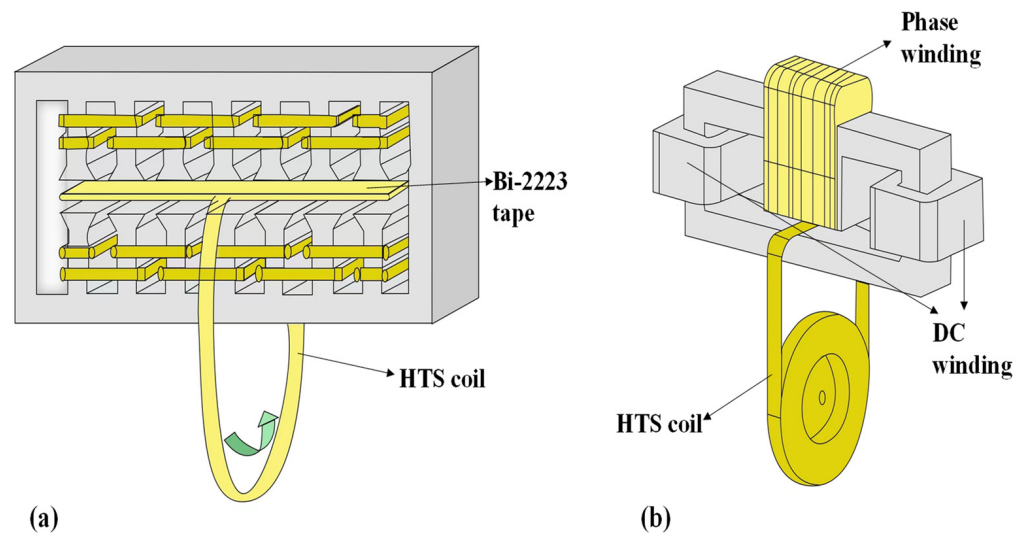
5. Other HTS Flux Pumps

The main categories of HTS flux pumps were substantially detailed in Sections 3 and 4; this section aims to provide readers with a wider overview of HTS flux pumps, by presenting several variants.

As mentioned earlier, Coombs et al. constructed a rig to magnetize YBCO samples [47–49]. In their experiments, they conjoined soft magnetic materials with hard ones in the flux path, as shown in Figure 15. The soft magnetic materials (e.g., Prussian Blue puck) undergo a change in permeability and the hard ones (e.g., permanent magnet NdFeB) undergo changes in magnetization when their temperature changes. As a combinational effect, magnetic pulses can be generated to travel over the surface of the superconductors. Technically, the operation principles are similar to the later conceived travelling wave HTS flux pumps. This type of thermal actuated HTS flux pumps have not been further developed, due to the challenges faced in operation. However, it is of great significance since it firstly realized flux pumping for HTSCs without any break of superconductivity.
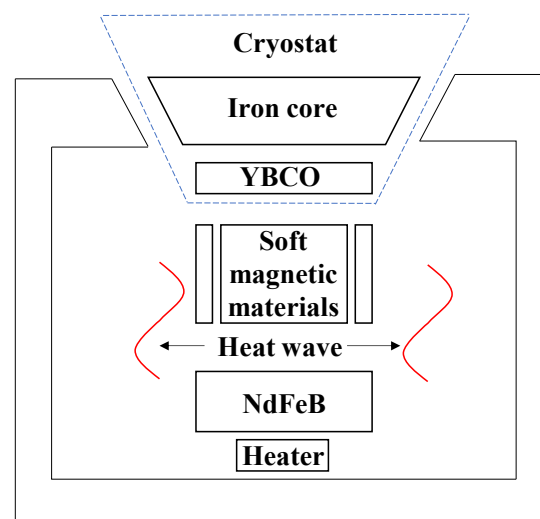
Figure 15. Illustration of the experimental set up for a thermal actuated HTS flux pump. Adapted from [48].

In [125–129], Bai et al. proposed a pulse-type magnetic flux pump to magnetize Bi-2223 tapes, as shown in Figure 16a. In their design, an HTS film is placed in the middle of a set of aligned solenoids and connected to an HTS loop. By controlling the input current, the solenoids can generate specific magnetic pulses over the HTS film, after which flux can be driven into the superconducting loop. This is again very similar to the travelling wave HTS flux pumps, especially the linear ones. Nevertheless, according to their explanation, the pulses are utilized to create a local normal region in the HTS film, which makes it totally different from all HTS flux pumps discussed above but resembles an LTS flux pump. Considering their experimental configurations, the solenoids with 300 turns are energized with a current below 2.5 A with 300 turns. Such an excitation is unlikely to produce a magnetic field strong enough to break the superconductivity for HTSCs, this is essentially a variant of the travelling wave HTS flux pump.

Figure 16. (**a**) Structure diagram of a pulse-type HTS flux pump. Adapted from [125]. (**b**) Experimental configuration of the linear HTS flux pump. Adapted from [130].

Refs. [130–133] claimed that they have designed a novel flux pump device to charge an HTS double pancake coil, as shown in Figure 16b. The only acting component is the static electromagnet, and thus it is referred to as a linear HTS flux pump in [133]. However, it should be noted according to the topology, that the magnetic core directly passes through the closed superconducting loop, which intuitively forms a transformer with the superconducting loop serving as the secondary winding. From this point of view, the situation becomes tricky since the charging current can likely result from direct electromagnetic induction, rather than flux pumping. The flux pumping effect reported in [130] can be well accounted for by Faraday's law: the injected DC current in the static electromagnet has led to the occurrence of the DC magnetic flux inside the HTS loop despite a short step-variation period. It should be noted that the initial magnetic flux inside the HTS loop is zero. Given the flux conservation characteristics and nearly zero resistance of a superconducting loop, a permanent circulating DC current will be induced to force the total magnetic flux inside the HTS coil to be zero [134]. As a result, a DC current can be generated in the HTS loop.

The transformer-rectifier HTS flux pumps discussed in Section 4 all rely on the HTS bridge to demonstrate temporary resistivity during each cycle of operation. Gawith et al. [135] proposed a double AC field switched flux pump, where an extra field is applied to part of the loop1 path in Figure 11. They pointed out that for a single AC field switched transformer-rectifier HTS flux pump, the resistance in loop1 is not zero even if the HTS bridge is superconducting, because there are fixed resistances due to circuit joints and the AC loss mechanism. Adding an extra AC field switch can help modulate the resistance in loop1 and potentially improve the performance compared to the single switch case. Alternatively, except for exploiting peculiar properties of superconductors, one can replace HTS switches with electronics devices, such as MOSFETs, which demonstrates high impedance during on-state and very low impedance during off-state [56]. In addition, the critical current density of HTS materials is associated with external magnetic field. Therefore, for a self-regulating transformer HTS flux pump, one can exploit the field dependence of critical current density to reduce the threshold of flux flow regime, which has proved helpful for improving efficiency [136].

6. Discussion

Based on the above analysis, it can be concluded that the creation of a resistive region without breaking the superconductivity in the whole HTS tape is the key to achieving

the DC output voltage. In other words, the non-linear dynamic resistance caused by the hysteretic and flux flow effect is the root for all types of HTS flux pumps. The functionality of all types of HTS flux pumps presented in this work is essentially achieved by the same working principle: an effective homopolar voltage is induced across a section of HTS tape, which can energize the charging loop by constantly ramping up current in it. For travelling wave HTS flux pumps, either rotating PMs or stationary electromagnets can be employed to provide the magnetic field required by the HTS tape to output a DC voltage. The core is to create highly unbalanced resistivity along the width of the HTS tape (due to the highly non-linear resistivity property), so whether the wave is "traveling" is not decisive. Applying a simple standing waveform can also lead to a measurable DC output, as long as the magnetic field is asymmetric in the time domain and spatially inhomogeneous. For transformer-rectifier HTS flux pumps, two options are available for triggering the resistivity in the HTS bridge, either by external AC magnetic fields or over-critical currents.

In terms of the fundamental physics, the two main categories (travelling wave and transformer-rectifier type) of HTS flux pumps are closely related and share common characteristics. In all cases of operating HTS flux pumps, the HTS bridge should be able to transport current greater than that carried in the load coil. This is automatically fulfilled, considering the load coil usually experiences a much higher field than the bridge. Otherwise, one would have to manually adjust the current capacity for the HTS bridge and load coil. One possible way to achieve that is to operate the HTS bridge at lower temperature than the load coil. Each of these devices requires only a small amount of supply to produce any desired level of current, while the limit is imposed by the maximum current that can be carried by the HTS load (i.e., the critical current). To scale up the pumped current level, one needs to increase the load current capacity.

Meanwhile, due to the distinctive topologies, there are critical differences between the two types of HTS flux pumps. As shown in Figure 3, the entire charging process occurs in one single loop, which means that the magnetic induction and switching are tightly coupled in a traveling wave HTS flux pump. This makes it difficult to mitigate the loss, because the transport current will always need to flow through the resistive HTS path. Yet, for a transformer-rectifier HTS flux pump, as shown in Figure 11, the charging current and transport current are separated. Hence, it is possible to suppress the loss, at least, by independently minimizing the off-state loss (e.g., when the applied field is removed). There is a sort of trade-off between the two types of HTS flux pumps, while the travelling wave HTS flux pump has the simplest structure and requires the least superconducting materials, the transformer-rectifier HTS flux pump possesses more flexibility and can possibly maintain lower loss.

Both of the two categories of HTS flux pumps support reversable operations. To invert the load, one can simply flip the wave propagation direction for a travelling wave HTS flux pump. By controlling whether the resistivity is triggered in the positive or negative half cycle of the secondary current, similar inversion effect can be achieved for a transformer-rectifier HTS flux pump. A comparison between different types of HTS flux pumps is presented in Table 1.

It should be pointed out that the definition of an HTS flux pump in the scope of this work is a device that can achieve flux pumping without breaking superconductivity in HTSCs at any given time during operation. In order to provide the most intuitive explanations for specific types of HTS flux pumps, the working mechanisms for typical variants of the HTS flux pump were separately introduced in Sections 3 and 4. However, we must emphasize again that the underlying physics is united, all of which point to the same principle, namely that a non-linear resistivity needs to be stimulated. More precisely, the AC-switched transformer-rectifier HTS flux pumps directly utilize the dynamic resistance that occurs when HTSCs carrying DC currents are exposed to external AC fields. The non-linear resistivity theory for travelling wave HTS flux pumps is essentially based on the *E-J* power law, the same as for the self-regulating transformer HTS flux pump which can be interpreted as an alternative manifestation of dynamic resistance.

Table 1. Comparison between major HTS flux pump categories.

Type	Pros	Cons	Notes
Rotary HTS flux pump	Simplest structure, easiest operation, least material consumption.	Mechanical drive is required to create relative motion between static and moving parts.	Losses are presented and difficult to mitigate due to the single loop topology.
Linear HTS flux pump	Concise configuration. The external field can be tuned easily.	Magnetic framework is required to divert flux path.	
AC field switched transformer-rectifier	The flux pumping process consists of several independent steps, thus highly flexible.	The system is sophisticated and imposes many operational considerations.	Losses are presented but can be modulated since the transport current and charging current are separated.
Self-regulating transformer-rectifier	It can operate at completely current-driven mode without any external field involved.	Potentially unstable due to the sharp *E-J* relation.	
Power electronics switched	Power electronics devices such as MOSFETs, IGBTs are cheap and widely available.	Commonly in power electronics devices, the on-state resistance is inevitable.	The operating frequency and output ripple are highly associated with electronics device standards.

Note: None of these HTS flux pumps need to break superconductivity during operation.

7. Applications

As previously mentioned in the paper, HTS flux pumps provide a promising solution for efficient load energization. One the one hand, it obviates the need for physical current leads, which not only simplifies the structural layout but also dramatically relieves the thermal load imposed on the cryogenic system. On the other hand, very high current can be obtained by repeatedly applying a small field without involving expensive and bulky power supplies, saving considerable capital cost. These unique merits are exceedingly attractive in a wide range of applications, including but not limited to electrical machines, ultra-high field magnets, MRI/NMR, generally wherever high current and/or high magnetic field are demanded.

In the electrical machine domain, the rotary HTS flux pumps are considered as congenitally beneficial, because they can take advantage of the inherent motion between the rotor and stator in an electric machine to achieve flux pumping. By applying rotary HTS flux pumps to energize field windings, neither slip rings or brushes are required, which are major sources of failure in an electric machine. In [32], Sung et al. outlined the design and heat analysis of a 12 MW HTS wind power generator module employing an HTS dynamo. The results have shown that total heat loss can be maintained at 39 W when the coil supporter adopts zigzag or pole shapes. The GM cryocooler has 50 W thermal capacity for the HTS coils to be operated at a temperature under 20 K, so the application of a rotary HTS flux pump in this wind power generator demonstrates clear feasibility [137]. In [31,138], the design was experimentally verified by fabricating Double Pancake Coils (DPCs) for the rotor poles of a 10 kW, 200 rpm wind power generator prototype. It was reported that the field windings can be energized to 1.5 T field through the injection of 85 A per pole. Research groups in Korea have proposed a structural design for a 12 MW HTS generator employing rotary HTS flux pumps in [139], where all the HTS field windings are structurally separated as shown in Figure 17a. Each HTS module coil consists of several components, including HTS field coils, coil bobbins, bobbin supports, a heat exchanger, a flux pump, a cryostat, and a cryo-cooler. The flux pump exciters located in each module are defined as rotating and stationary parts as shown in Figure 17b (similar to the flux pumping part and charging part in Figure 3a). The rotating parts are rotated by interlocking gear teeth of the generator and flux pump exciter, while the stationary parts are included in the cryostat of the coil module to directly connect the HTS field coil with HTS stator wire. A more recent work published by Kalsi et al. [140] described a 2 MW, 25,000 rpm concept design for homopolar superconducting AC machines, with rotary HTS flux pump driven field coils, for aerospace applications. The design was inspired by the General Electric's Homopolar Inductor Alternator (HIA) prototype [4], achieving a power density

of ~9 kW/kg for a 5MWA, 35,000 rpm machine. Machines of this type are an ideal choice for future aerospace applications, because both the AC armature and DC excitations are included within the stationary part of the machine, as shown in Figure 18a. A solid steel rotor is magnetized by the stationary excitation winding, so that the operating speed is limited only by the mechanical stress limit of the rotor steel. The rotary HTS flux pump to be integrated with the circular coil is shown in Figure 18b, which is capable of managing field current in the range of 188–364 A. Following the preliminary charging test of HTS coils for the rotor field winding of a 1-kW-class HTS rotating machine [141,142], the world's first implementation of an HTS machine that employs an HTS rotary flux pump as the exciter has been reported in [143]. A maximum output power of 1779 W has been successfully obtained, with the rotating speed of 600 rpm, field current of 1.72 A, and average three phase load of 203 ohms. The excitation loss (for field current below the saturated value at 100 A) was estimated to be 1.11 W, which is approximately 91.5% less than those of the two pairs of copper current leads.
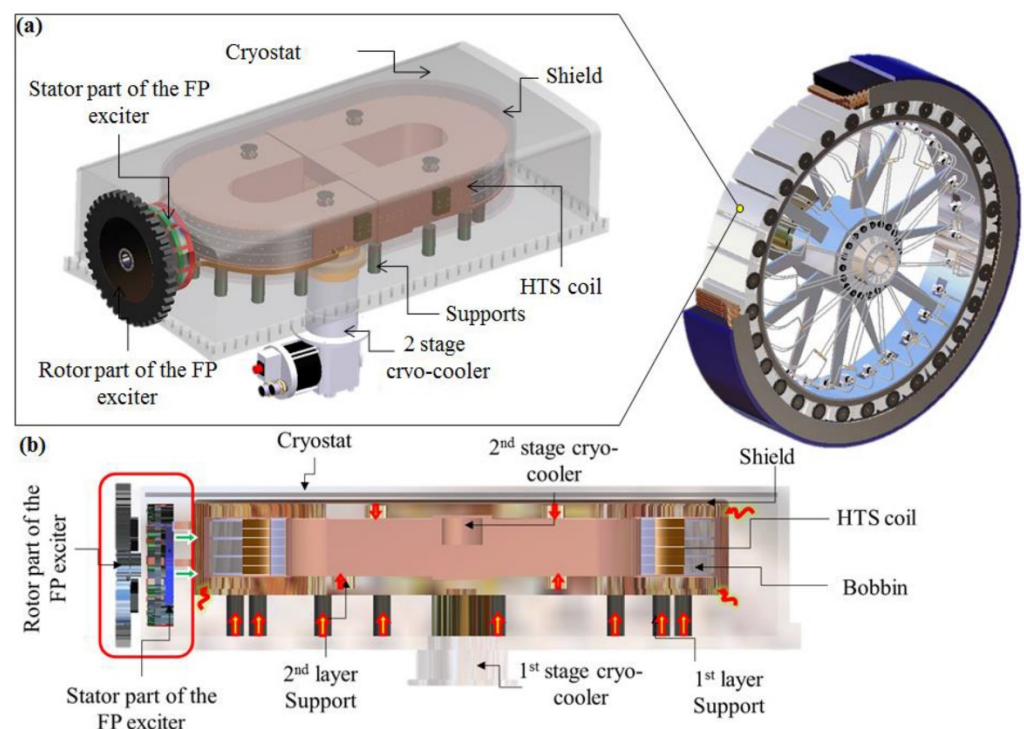
Figure 17. Configuration of the rotary HTS flux pump-based module coil. (**a**) overview (**b**) cross section view, of a separated unit of HTS field coils. Reprinted from [139].
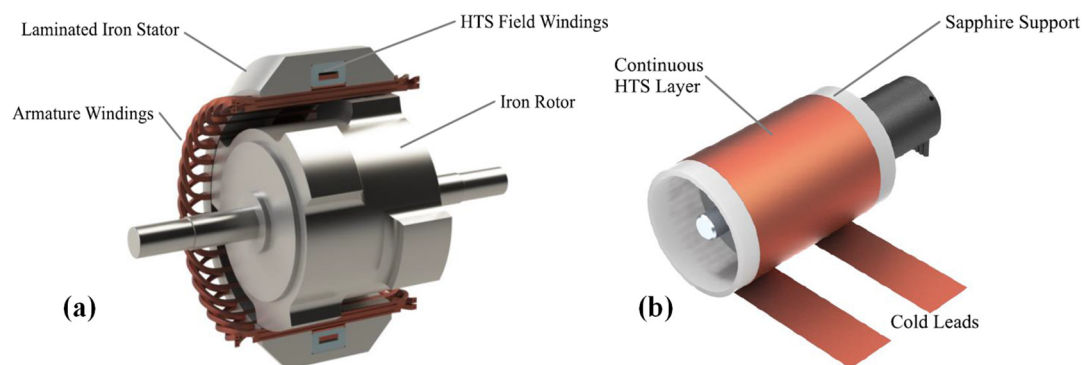
Figure 18. (**a**) Sectioned view of the AC homopolar motor/generator, (**b**) rotary HTS flux pump concept to be integrated with the field coil. Reprinted from [140].

Superconducting technology has boosted MRI/NMR advancement over past decades, by the means of providing high magnetic fields that are not available from conventional magnets. MRI/NMR equipment requires the continuous production of a large homogenous field, typically 1–7 T. The state-of-the-art technology employs LTSCs, which need to cool down to liquid helium temperature 4.2 K. It is rather evident that LTSCs for current MRI/NMR technology are reaching their bottlenecks and new developments such as obtaining higher fields and reducing operational costs are in favor of HTSCs [144–147]. HTSCs not only can operate at relatively elevated temperatures (typically 100 K or above), but also are able to withstand intensive magnetic field strength, which can theoretically go up to the orders of hundreds of Teslas in magnitude. The HTS flux pump technologies, with the advantage of reliving thermal load, offer additional benefits by enabling much more compact structure. The electromagnetic design of a 1.5 T REBCO magnet for dedicated MRI has been presented in [148]. By applying no-insulation linear HTS flux pump technology, the magnet was contained within a compact volume; the outer diameter and axial length are both less than 300 mm, diameter of the room-temperature bore is 200 mm. Moreover, the superconductor consumption can be greatly saved by 29.7% via employing multiple HTS flux pumps as the excitation sources. The idea of constructing a compact and mobile HTS MRI head scanner has been reported in [149], in which a half-bridge transformer-rectifier type HTS flux pump is employed to induce current in the form of triangular waves at a near DC frequency (5–10 Hz). The industrial design guidelines for conduction cooled MRI magnets using NbTi are presented in Table 2, from where HTS flux pumps see clear potential to be utilized for MRI magnets within existing guidelines, allowing higher operating temperature and lower cost.

Table 2. MRI magnet design guidelines [150].

Strength	1.5 T	3.0 T	7.0 T
Operating temperature (K)	4.2	4.2	4.2
Amount of LHe (L)	1700	<3000	4000
Length including 10 cm for cryogenics (m)	1.25–1.70	1.60–1.80	3.0
Stored energy (MJ)	2–4	10–15	50–90
Peak magnetic field * (T)	<9	<9	<9
Coil operating current density * (A/mm^2)	<250	<250	<250
Ampere-length (kA-km)	15–25	35–60	120–180

* The NbTi wire has a critical density of 250 A/mm^2 at peak magnetic field strength of 9 T measured at 1.2 K [151].

For ultra-high field magnets required for diverse scientific and industrial uses, it has been validated that high-field copper oxide superconductor magnets can break through the top limit set by LTSCs [152]. In such cases, HTS flux pumps are also ideal candidates for providing either the background field of the direct-current hybrid magnets [153] or the desired field directly. As already discussed above, HTS flux pumps can be driven by a small magnetic field to energize the load coils, and the charging cycle can be continuously repeatedly. In other words, any desired currents, thus equivalent magnetic fields, are achievable, whilst the limitations are only imposed by the HTSCs current transport capacity and inherent losses. A quasi-persistent current of over 1.1 kA has been achieved using an AC field switched transformer-rectifier HTS flux pump, maintaining high flux injection accuracy with an overall flux ripple of less than 0.2 milli-Weber [113]. The record was broken soon afterwards when a maximum pumped current greater than 2 kA was reported in [116], utilizing a self-regulating HTS flux pump. In such a device, over 1 kA current was still achievable even with a 6.8 mm airgap incorporated into the steel transformer core. Judging from existing developments, it is promising that the HTS flux pump can play a key role in ultra-high field magnets.

8. Conclusions

Essentially, HTS flux pumps are enabled by the dynamic resistance caused by the hysteretic and flux flow effects. Despite remarkable progress being achieved in HTS flux pumps in different perspectives, there are some areas that are relatively overlooked and can be further improved. Based on our understanding, we highlight three of them here:

- Most work on HTS flux pumps presented in the current literature focuses on operational research and theoretical analysis, namely, how to increase the pumped current and figure out the underlying mechanism. Limited attention has been put on the losses associated with HTS flux pumps [154], which directly determines the efficiency of the flux pump system. The scenario, where conducting superconductors are exposed to external AC fields, appears in almost all HTS flux pumps, which means certain AC losses must exist [155–157]. Especially for the AC field switched transfer-rectifier HTS flux pump, in which their working principles are essentially based on AC losses. Moreover, in order to scale up the pumped current, one will need to solder multiple HTS loads together with multiple HTS bridges (switches). As a result, it is inevitable that extra heat losses due to non-zero joint resistances will be produced [113]. A recent work [158] has described the energy balance for HTS dynamos, in which it was demonstrated that due to the interactions of induced currents with rotating PMs, a significant part of the mechanical power supplied to the rotor is converted into Joule dissipation with HTSCs. If these losses are not well modulated, the HTS components may be placed at the risk of quenching, which will result in failure of the whole system.
- The most obvious criterion to evaluate the performance of an HTS flux pump is the output voltage (in open circuit condition) or pumping current (in closed loop condition). Ideally, we want the output to be as high as possible. However, it should be highlighted that the peak of the output is not the only concern. In many cases, the ripple plays a critical role. For instance, in a synchronous machine, if the excitation current in field winding is not maintained constant, the electromagnetic force generated by the external rotating field changes accordingly, which will cause output fluctuation or even fatal damage to the machine. Due to external vibrations, such as noise from the input system, ripples can be expected in any type of HTS flux pump. In particular, the self-regulating transfer-rectifier flux pump is operated in the flux flow regime (sharp *E-J* relation), where a small turbulence in the current can result in very large ripples. Hence, it is necessary to integrate a reliable control system to HTS flux pumps to stabilize the output. The authors of [159,160] proposed a proportion–integral–differential (PID) loop for a rotary HTS flux pump and [161] demonstrated a feedback circuit for a transformer-rectifier flux pump, both showing great effectiveness for smoothing the output ripple. A sensitive control system is desired for more sophisticated applications.
- One of the key obstacles that hinders the advancement of the HTS flux pump is the operating cost. The HTS components, which are not cheap themselves, plus the expensive compulsory cryogenic system make the construction and operation of such devices costly. Alternatively, accurate simulation can be utilized to investigate HTS flux pumps without undertaking real experiments, saving substantial costs. The modeling of HTS flux pumps has mainly relied on FEM models, which are extremely helpful for acquiring details about the electromagnetic behavior involved in HTS flux pumps. However, FEM models are often time consuming, because they need to mathematically simulate the whole process to replicate the real case. Moreover, FEM models require users to have abundant knowledge about the problem they are modeling. These features are absolutely not preferred from the perspective of industrial design and optimization, where the interests will be capturing certain specifications that can evaluate the device performance rather than delving into the underlying physics. Recent work in [69] proposed an innovative statistical model based on machine learning techniques, for capturing the output characteristics of a rotary HTS flux pump. In that model, the output voltage can be immediately

predicted according to several design parameters with very high accuracy. Such machine learning enabled models can be further developed, which are expected to become powerful design tools for HTS flux pumps and other superconducting applications.

In summary, the HTS flux pump is a promising technology for contactless energization, with higher efficiency, lower cost, and more compact size. In practical scenarios, HTS flux pumps provide general advantages for designing more flexible MRI/NMR with reduced cost. The travelling wave HTS flux pumps, especially the rotary type, show clear attractions for the next generation of electric machines, where high power density is demanded. The transformer-rectifier type of HTS flux pumps possess considerable scale up possibility, which are very promising for the development of ultra-high magnets. It is reasonable to expect that HTS flux pumps will become an enabling technology in various industrial sectors. In brief, all existing HTS flux pumps have been presented in detail, illustrating their design, physical mechanism, operational characteristics, as well as modeling methods. Proposals have been put forward to address potential concerns for future development. In this paper, the authors provided an in-depth insight into the HTS flux pump technology in order to inspire further advances in the technology.

References

1. Weijers, H.; Trociewitz, U.; Markiewicz, W.; Jiang, J.; Myers, D.; Hellstrom, E.; Xu, A.; Jaroszynski, J.; Noyes, P.; Viouchkov, Y. High field magnets with HTS conductors. *IEEE Trans. Appl. Supercond.* **2010**, *20*, 576–582. [CrossRef]
2. Hahn, S.; Park, D.K.; Voccio, J.; Bascunan, J.; Iwasa, Y. No-Insulation (NI) HTS Inserts for > 1 GHz LTS/HTS NMR Magnets. *IEEE Trans. Appl. Supercond.* **2011**, *22*, 4302405. [CrossRef] [PubMed]
3. Abrahamsen, A.B.; Mijatovic, N.; Seiler, E.; Zirngibl, T.; Træholt, C.; Nørgård, P.B.; Pedersen, N.F.; Andersen, N.H.; Østergaard, J. Superconducting wind turbine generators. *Supercond. Sci. Technol.* **2010**, *23*, 034019. [CrossRef]
4. Sivasubramaniam, K.; Zhang, T.; Lokhandwalla, M.; Laskaris, E.; Bray, J.; Gerstler, B.; Shah, M.; Alexander, J. Development of a high speed HTS generator for airborne applications. *IEEE Trans. Appl. Supercond.* **2009**, *19*, 1656–1661. [CrossRef]
5. Miki, M.; Tokura, S.; Hayakawa, H.; Inami, H.; Kitano, M.; Matsuzaki, H.; Kimura, Y.; Ohtani, I.; Morita, E.; Ogata, H. Development of a synchronous motor with Gd–Ba–Cu–O bulk superconductors as pole-field magnets for propulsion system. *Supercond. Sci. Technol.* **2006**, *19*, S494. [CrossRef]
6. Umemoto, K.; Aizawa, K.; Yokoyama, M.; Yoshikawa, K.; Kimura, Y.; Izumi, M.; Ohashi, K.; Numano, M.; Okumura, K.; Yamaguchi, M. Development of 1 MW-class HTS motor for podded ship propulsion system. *J. Phys. Conf. Ser.* **2010**, *234*, 032060. [CrossRef]
7. Nick, W.; Frank, M.; Klaus, G.; Frauenhofer, J.; Neumuller, H.-W. Operational experience with the world's first 3600 rpm 4 MVA generator at Siemens. *IEEE Trans. Appl. Supercond.* **2007**, *17*, 2030–2033. [CrossRef]
8. Sung, H.-J.; Kim, G.-H.; Kim, K.; Jung, S.-J.; Park, M.; Yu, I.-K.; Kim, Y.-G.; Lee, H.; Kim, A.-R. Practical design of a 10 MW superconducting wind power generator considering weight issue. *IEEE Trans. Appl. Supercond.* **2013**, *23*, 5201805. [CrossRef]
9. Karmaker, H.; Ho, M.; Chen, E.; Kulkarni, D. Direct drive HTS wind generator design for commercial applications. In Proceedings of the 2014 International Conference on Electrical Machines (ICEM), Berlin, Germany, 2–5 September 2014; pp. 491–495.

10. Sung, H.-J.; Kim, G.-H.; Kim, K.; Park, M.; Yu, I.-K.; Kim, J.-Y. Design and comparative analysis of 10 MW class superconducting wind power generators according to different types of superconducting wires. *Phys. C Supercond.* **2013**, *494*, 255–261. [CrossRef]

11. Filipenko, M.; Kühn, L.; Gleixner, T.; Thummet, M.; Lessmann, M.; Möller, D.; Böhm, M.; Schröter, A.; Häse, K.; Grundmann, J. Concept design of a high power superconducting generator for future hybrid-electric aircraft. *Supercond. Sci. Technol.* **2020**, *33*, 054002. [CrossRef]

12. Boll, M.; Corduan, M.; Biser, S.; Filipenko, M.; Pham, Q.H.; Schlachter, S.; Rostek, P.; Noe, M. A holistic system approach for short range passenger aircraft with cryogenic propulsion system. *Supercond. Sci. Technol.* **2020**, *33*, 044014. [CrossRef]

13. Lvovsky, Y.; Stautner, E.W.; Zhang, T. Novel technologies and configurations of superconducting magnets for MRI. *Supercond. Sci. Technol.* **2013**, *26*, 093001. [CrossRef]

14. Corato, V.; Bagni, T.; Biancolini, M.; Bonifetto, R.; Bruzzone, P.; Bykovsky, N.; Ciazynski, D.; Coleman, M.; Della Corte, A.; Dembkowska, A. Progress in the design of the superconducting magnets for the EU DEMO. *Fusion Eng. Des.* **2018**, *136*, 1597–1604. [CrossRef]

15. Zhang, M.; Yuan, W.; Hilton, D.K.; Canassy, M.D.; Trociewitz, U.P. Study of second-generation high-temperature superconducting magnets: The self-field screening effect. *Supercond. Sci. Technol.* **2014**, *27*, 095010. [CrossRef]

16. Khodzhibagiyan, H.; Agapov, N.; Akishin, P.; Blinov, N.; Borisov, V.; Bychkov, A.; Galimov, A.; Donyagin, A.; Karpinskiy, V.; Korolev, V. Superconducting magnets for the NICA accelerator collider complex. *IEEE Trans. Appl. Supercond.* **2013**, *24*, 4001304. [CrossRef]

17. Rossi, L. Superconducting magnets for the LHC main lattice. *IEEE Trans. Appl. Supercond.* **2004**, *14*, 153–158. [CrossRef]

18. Yokoyama, K.; Oka, T.; Okada, H.; Fujine, Y.; Chiba, A.; Noto, K. Solid-liquid magnetic separation using bulk superconducting magnets. *IEEE Trans. Appl. Supercond.* **2003**, *13*, 1592–1595. [CrossRef]

19. Tomita, M.; Murakami, M. High-temperature superconductor bulk magnets that can trap magnetic fields of over 17 tesla at 29 K. *Nature* **2003**, *421*, 517–520. [CrossRef]

20. Durrell, J.H.; Dennis, A.R.; Jaroszynski, J.; Ainslie, M.D.; Palmer, K.G.; Shi, Y.; Campbell, A.M.; Hull, J.; Strasik, M.; Hellstrom, E. A trapped field of 17.6 T in melt-processed, bulk Gd-Ba-Cu-O reinforced with shrink-fit steel. *Supercond. Sci. Technol.* **2014**, *27*, 082001. [CrossRef]

21. Patel, A.; Baskys, A.; Mitchell-Williams, T.; McCaul, A.; Coniglio, W.; Hänisch, J.; Lao, M.; Glowacki, B.A. A trapped field of 17.7 T in a stack of high temperature superconducting tape. *Supercond. Sci. Technol.* **2018**, *31*, 09LT01. [CrossRef]

22. Toth, J.; Bole, S. Design, construction, and first testing of a 41.5 T all-resistive magnet at the NHMFL in Tallahassee. *IEEE Trans. Appl. Supercond.* **2017**, *28*, 4300104. [CrossRef]

23. Iijima, Y.; Kaneko, N.; Hanyu, S.; Sutoh, Y.; Kakimoto, K.; Ajimura, S.; Saitoh, T. Development of IBAD/PLD process for long length Y-123 conductors in Fujikura. *Phys. C Supercond. Appl.* **2006**, *445*, 509–514. [CrossRef]

24. Freyhardt, H.C. YBaCuO and REBaCuO HTS for applications. *Int. J. Appl. Ceram. Technol.* **2007**, *4*, 203–216. [CrossRef]

25. Shiohara, Y.; Yoshizumi, M.; Izumi, T.; Yamada, Y. Present status and future prospect of coated conductor development and its application in Japan. *Supercond. Sci. Technol.* **2008**, *21*, 034002. [CrossRef]

26. Sugano, M.; Osamura, K.; Prusseit, W.; Semerad, R.; Kuroda, T.; Itoh, K.; Kiyoshi, T. Reversible strain dependence of critical current in 100 A class coated conductors. *IEEE Trans. Appl. Supercond.* **2005**, *15*, 3581–3584. [CrossRef]

27. Lee, J.-H.; Lee, H.; Lee, J.-W.; Choi, S.-M.; Yoo, S.-I.; Moon, S.-H. RCE-DR, a novel process for coated conductor fabrication with high performance. *Supercond. Sci. Technol.* **2014**, *27*, 044018. [CrossRef]

28. Ballarino, A. Current leads, links and buses. *arXiv* **2015**, arXiv:1501.07166.

29. Wegener, L. Status of Wendelstein 7-X construction. *Fusion Eng. Des.* **2009**, *84*, 106–112. [CrossRef]

30. Ballarino, A. Current leads for the LHC magnet system. *IEEE Trans. Appl. Supercond.* **2002**, *12*, 1275–1280. [CrossRef]

31. Bumby, C.W.; Badcock, R.A.; Sung, H.-J.; Kim, K.-M.; Jiang, Z.; Pantoja, A.E.; Bernardo, P.; Park, M.; Buckley, R.G. Development of a brushless HTS exciter for a 10 kW HTS synchronous generator. *Supercond. Sci. Technol.* **2016**, *29*, 024008. [CrossRef]

32. Sung, H.; Badcock, R.; Jiang, Z.; Choi, J.; Park, M.; Yu, I. Design and heat load analysis of a 12 MW HTS wind power generator module employing a brushless HTS exciter. *IEEE Trans. Appl. Supercond.* **2016**, *26*, 5205404. [CrossRef]

33. Jeon, H.; Lee, J.; Han, S.; Kim, J.H.; Hyeon, C.J.; Kim, H.M.; Park, D.; Do Chung, Y.; Ko, T.K.; Yoon, Y.S. Methods for increasing the saturation current and charging speed of a rotary HTS flux-pump to charge the field coil of a synchronous motor. *IEEE Trans. Appl. Supercond.* **2018**, *28*, 5202605. [CrossRef]

34. Kalsi, S.S. *Applications of High Temperature Superconductors to Electric Power Equipment*; John Wiley & Sons: Hoboken, NJ, USA, 2011.

35. Feigel'man, M.; Geshkenbein, V.; Vinokur, V. Flux creep and current relaxation in high-T c superconductors. *Phys. Rev. B* **1991**, *43*, 6263. [CrossRef] [PubMed]

36. Hildebrandt, A.F.; Wahlquist, H.; Elleman, D.D. Configurations of superconducting shells required for near critical uniform magnetic fields. *J. Appl. Phys.* **1962**, *33*, 1798–1800. [CrossRef]

37. Hildebrandt, A.F.; Elleman, D.D.; Whitmore, F.C.; Simpkins, R. Some Experimental Consequences of Flux Conservation within Multiply-Connected Superconductors. *J. Appl. Phys.* **1962**, *33*, 2375–2377. [CrossRef]

38. Rose-Innes, A. A superconducting magnetic flux compressor. *Cryogenics* **1973**, *13*, 103–105. [CrossRef]

39. Van Beelen, H.; AJPT Arnold, M.; Sypkens, H.; De Bruyn Ouboter, R.; Beenakker, J.; Taconis, K. A 25 000 gauss, 175 amperes Nb-25% Zr wire magnet fed by a flux pump. *Phys. Lett.* **1963**, *7*. [CrossRef]

40. Van Suchtelen, J.; Volger, J.; Van Houwelingen, D. The principle and performance of a superconducting dynamo. *Cryogenics* **1965**, *5*, 256–266. [CrossRef]

41. Van Beelen, H.; Houckgeest, J.V.B.; Ouboter, R.D.B.; Taconis, K. Remarks on a moving-flux experiment in superconducting sheets. *Physica* **1967**, *36*, 107–117. [CrossRef]

42. Atherton, D. High-Efficiency Superconducting Homopolar dc Generators. *J. Appl. Phys.* **1968**, *39*, 2639. [CrossRef]

43. Van Beelen, H.; De Langen, M.; Kerkdijk, C. Comments on the efficiency of flux pumping into superconducting circuits. *Physica* **1969**, *42*, 265–276. [CrossRef]

44. Purcell, J.; Payne, E. Superconducting rectifiers. In *Advances in Cryogenic Engineering*; Springer: Berlin/Heidelberg, Germany, 1961; pp. 149–153.

45. Hempstead, C.; Kim, Y.; Strnad, A. Inductive behavior of superconducting magnets. *J. Appl. Phys.* **1963**, *34*, 3226–3236. [CrossRef]

46. Buchhold, T. Superconductive power supply and its application for electrical flux pumping. *Cryogenics* **1964**, *4*, 212–217. [CrossRef]

47. Coombs, T.; Hong, Z.; Zhu, X. A thermally actuated superconducting flux pump. *Phys. C Supercond.* **2008**, *468*, 153–159. [CrossRef]

48. Coombs, T.; Hong, Z.; Yan, Y.; Rawlings, C. The next generation of superconducting permanent magnets: The flux pumping method. *IEEE Trans. Appl. Supercond.* **2009**, *19*, 2169–2173. [CrossRef]

49. Yan, Y.; Li, Q.; Coombs, T. Thermally actuated magnetization flux pump in single-grain YBCO bulk. *Supercond. Sci. Technol.* **2009**, *22*, 105011. [CrossRef]

50. Coombs, T.A.; Geng, J.; Fu, L.; Matsuda, K. An overview of flux pumps for HTS coils. *IEEE Trans. Appl. Supercond.* **2016**, *27*, 4600806. [CrossRef]

51. Coombs, T. Superconducting flux pumps. *J. Appl. Phys.* **2019**, *125*, 230902. [CrossRef]

52. Zhai, Y.; Tan, Z.; Liu, X.; Shen, B.; Coombs, T.A.; Wang, F. Research Progress of Contactless Magnetization Technology: HTS Flux Pumps. *IEEE Trans. Appl. Supercond.* **2020**, *30*, 4602905. [CrossRef]

53. Van de Klundert, L.; ten Kate, H.H. Fully superconducting rectifiers and fluxpumps Part 1: Realized methods for pumping flux. *Cryogenics* **1981**, *21*, 195–206. [CrossRef]

54. van de Klundert, L.; ten Kate, H. On fully superconducting rectifiers and fluxpumps. A review. Part 2: Commutation modes, characteristics and switches. *Cryogenics* **1981**, *21*, 267–277. [CrossRef]

55. Mulder, G.; Ten Kate, H.; Krooshoop, H.; van de Klundert, L. Development of a thermally switched superconducting rectifier for 100 kA. *IEEE Trans. Magn.* **1991**, *27*, 2333–2336. [CrossRef]

56. Oomen, M.P.; Leghissa, M.; Ries, G.; Proelss, N.; Neumueller, H.-W.; Steinmeyer, F.; Vester, M.; Davies, F. HTS flux pump for cryogen-free HTS magnets. *IEEE Trans. Appl. Supercond.* **2005**, *15*, 1465–1468. [CrossRef]

57. Hoffmann, C.; Pooke, D.; Caplin, A.D. Flux pump for HTS magnets. *IEEE Trans. Appl. Supercond.* **2010**, *21*, 1628–1631. [CrossRef]

58. Hoffmann, C.; Walsh, R.; Karrer-Mueller, E.; Pooke, D. Design parameters for an HTS flux pump. *Phys. Procedia* **2012**, *36*, 1324–1329. [CrossRef]

59. Bumby, C.W.; Pantoja, A.E.; Sung, H.-J.; Jiang, Z.; Kulkarni, R.; Badcock, R.A. Through-wall excitation of a magnet coil by an external-rotor HTS flux pump. *IEEE Trans. Appl. Supercond.* **2016**, *26*, 0500505. [CrossRef]

60. Storey, J.G.; Pantoja, A.E.; Jiang, Z.; Hamilton, K.; Badcock, R.A.; Bumby, C.W. Impact of annular yoke geometry on performance of a dynamo-type HTS flux pump. *IEEE Trans. Appl. Supercond.* **2018**, *28*, 5203906. [CrossRef]

61. Pantoja, A.E.; Storey, J.G.; Badcock, R.A.; Jiang, Z.; Phang, S.; Bumby, C.W. Output during continuous frequency ramping of a dynamo-type HTS flux pump. *IEEE Trans. Appl. Supercond.* **2018**, *28*, 5202205. [CrossRef]

62. Storey, J.G.; Pantoja, A.E.; Jiang, Z.; Badcock, R.A.; Bumby, C.W. Optimizing rotor speed and geometry for an externally mounted HTS dynamo. *IEEE Trans. Appl. Supercond.* **2019**, *29*, 5202705. [CrossRef]

63. Jiang, Z.; Bumby, C.W.; Badcock, R.A.; Sung, H.-J.; Long, N.J.; Amemiya, N. Impact of flux gap upon dynamic resistance of a rotating HTS flux pump. *Supercond. Sci. Technol.* **2015**, *28*, 115008. [CrossRef]

64. Bumby, C.W.; Phang, S.; Pantoja, A.E.; Jiang, Z.; Storey, J.G.; Sung, H.-J.; Park, M.; Badcock, R.A. Frequency dependent behavior of a dynamo-type HTS flux pump. *IEEE Trans. Appl. Supercond.* **2016**, *27*, 5200705. [CrossRef]

65. Pantoja, A.E.; Jiang, Z.; Badcock, R.A.; Bumby, C.W. Impact of stator wire width on output of a dynamo-type HTS flux pump. *IEEE Trans. Appl. Supercond.* **2016**, *26*, 4805208. [CrossRef]

66. Badcock, R.A.; Phang, S.; Pantoja, A.E.; Jiang, Z.; Storey, J.G.; Sung, H.-J.; Park, M.; Bumby, C.W. Impact of magnet geometry on output of a dynamo-type HTS flux pump. *IEEE Trans. Appl. Supercond.* **2016**, *27*, 5200905. [CrossRef]

67. Zhang, H.; Yao, M.; Kails, K.; Machura, P.; Mueller, M.; Jiang, Z.; Xin, Y.; Li, Q. Modelling of electromagnetic loss in HTS coated conductors over a wide frequency band. *Supercond. Sci. Technol.* **2020**, *33*, 025004. [CrossRef]

68. Zhang, H.; Chen, H.; Jiang, Z.; Yang, T.; Xin, Y.; Mueller, M.; Li, Q. A full-range formulation for dynamic loss of high-temperature superconductor coated conductors. *Supercond. Sci. Technol.* **2020**, *33*, 05LT01. [CrossRef]

69. Wen, Z.; Zhang, H.; Mueller, M. Sensitivity analysis and machine learning modelling for the output characteristics of rotary HTS flux pumps. *Supercond. Sci. Technol.* **2021**, *34*, 125019. [CrossRef]

70. Mataira, R.; Ainslie, M.D.; Badcock, R.; Bumby, C.W. Modeling of Stator Versus Magnet Width Effects in High-T_c Superconducting Dynamos. *IEEE Trans. Appl. Supercond.* **2020**, *30*, 5204406. [CrossRef]

71. Fu, L.; Matsuda, K.; Baghdadi, M.; Coombs, T. Linear flux pump device applied to high temperature superconducting (HTS) magnets. *IEEE Trans. Appl. Supercond.* **2015**, *25*, 4603804. [CrossRef]

72. Fu, L.; Matsuda, K.; Lecrevisse, T.; Iwasa, Y.; Coombs, T. A flux pumping method applied to the magnetization of YBCO superconducting coils: Frequency, amplitude and waveform characteristics. *Supercond. Sci. Technol.* **2016**, *29*, 04LT01. [CrossRef]

73. Fu, L.; Matsuda, K.; Coombs, T. Linear flux pump device applied to HTS magnets: Further characteristics on wave profile, number of poles, and control of saturated current. *IEEE Trans. Appl. Supercond.* **2016**, *26*, 0500304. [CrossRef]

74. Fu, L.; Matsuda, K.; Shen, B.; Coombs, T. Charging an HTS Coil: Flux Pump With an HTS Square Bridge. *IEEE Trans. Appl. Supercond.* **2021**, *31*, 3800405. [CrossRef]

75. Coombs, T.; Fagnard, J.-F.; Matsuda, K. Magnetization of 2-G coils and artificial bulks. *IEEE Trans. Appl. Supercond.* **2014**, *24*, 8201005. [CrossRef]

76. Geng, J.; Matsuda, K.; Fu, L.; Fagnard, J.-F.; Zhang, H.; Zhang, X.; Shen, B.; Dong, Q.; Baghdadi, M.; Coombs, T. Origin of dc voltage in type II superconducting flux pumps: Field, field rate of change, and current density dependence of resistivity. *J. Phys. D Appl. Phys.* **2016**, *49*, 11LT01. [CrossRef]

77. Bumby, C.; Jiang, Z.; Storey, J.; Pantoja, A.; Badcock, R. Anomalous open-circuit voltage from a high-T c superconducting dynamo. *Appl. Phys. Lett.* **2016**, *108*, 122601. [CrossRef]

78. Mataira, R.; Ainslie, M.; Badcock, R.; Bumby, C. Origin of the DC output voltage from a high-Tc superconducting dynamo. *Appl. Phys. Lett.* **2019**, *114*, 162601. [CrossRef]

79. Mataira, R.; Ainslie, M.; Pantoja, A.; Badcock, R.; Bumby, C. Mechanism of the high-T c superconducting dynamo: Models and experiment. *Phys. Rev. Appl.* **2020**, *14*, 024012. [CrossRef]

80. Wang, W.; Coombs, T. Macroscopic magnetic coupling effect: The physical origination of a high-temperature superconducting flux pump. *Phys. Rev. Appl.* **2018**, *9*, 044022. [CrossRef]

81. Wei, J.; Wang, W.; Yang, Z.; Ye, H.; Zhang, Y.; Li, H.; Xu, H.; Shen, B.; Zhai, Y.; Zhou, Q. Build Charging Database of Linear-Motor Type Flux Pump and Analyze the Influence of DC-Bias Field Using Fixed Step Size Search Algorithm. *IEEE Trans. Appl. Supercond.* **2021**, *31*, 0500305. [CrossRef]

82. Kajikawa, K.; Hayashi, T.; Yoshida, R.; Iwakuma, M.; Funaki, K. Numerical evaluation of AC losses in HTS wires with 2D FEM formulated by self magnetic field. *IEEE Trans. Appl. Supercond.* **2003**, *13*, 3630–3633. [CrossRef]

83. Hong, Z.; Campbell, A.; Coombs, T. Numerical solution of critical state in superconductivity by finite element software. *Supercond. Sci. Technol.* **2006**, *19*, 1246. [CrossRef]

84. Brambilla, R.; Grilli, F.; Martini, L. Development of an edge-element model for AC loss computation of high-temperature superconductors. *Supercond. Sci. Technol.* **2006**, *20*, 16. [CrossRef]

85. Ainslie, M.D.; Yuan, W.; Hong, Z.; Pei, R.; Flack, T.J.; Coombs, T.A. Modeling and electrical measurement of transport AC loss in HTS-based superconducting coils for electric machines. *IEEE Trans. Appl. Supercond.* **2010**, *21*, 3265–3268. [CrossRef]

86. Ainslie, M.D.; Flack, T.J.; Campbell, A.M. Calculating transport AC losses in stacks of high temperature superconductor coated conductors with magnetic substrates using FEM. *Phys. C Supercond.* **2012**, *472*, 50–56. [CrossRef]

87. Brambilla, R.; Grilli, F.; Martini, L.; Bocchi, M.; Angeli, G. A finite-element method framework for modeling rotating machines with superconducting windings. *IEEE Trans. Appl. Supercond.* **2018**, *28*, 5207511. [CrossRef]

88. Santos, B.M.O.; Dias, F.J.M.; Sass, F.; Sotelo, G.G.; Polasek, A.; de Andrade, R. Simulation of superconducting machine with stacks of coated conductors using hybrid ah formulation. *IEEE Trans. Appl. Supercond.* **2020**, *30*, 5207309. [CrossRef]

89. Liang, F.; Venuturumilli, S.; Zhang, H.; Zhang, M.; Kvitkovic, J.; Pamidi, S.; Wang, Y.; Yuan, W. A finite element model for simulating second generation high temperature superconducting coils/stacks with large number of turns. *J. Appl. Phys.* **2017**, *122*, 043903. [CrossRef]

90. Zhang, H.; Zhang, M.; Yuan, W. An efficient 3D finite element method model based on the T–A formulation for superconducting coated conductors. *Supercond. Sci. Technol.* **2016**, *30*, 024005. [CrossRef]

91. Berrospe-Juarez, E.; Zermeño, V.M.; Trillaud, F.; Grilli, F. Real-time simulation of large-scale HTS systems: Multi-scale and homogeneous models using the T–A formulation. *Supercond. Sci. Technol.* **2019**, *32*, 065003. [CrossRef]

92. Grilli, F.; Pardo, E.; Morandi, A.; Gömöry, F.; Solovyov, M.; Zermeño, V.M.; Brambilla, R.; Benkel, T.; Riva, N. Electromagnetic modeling of superconductors with commercial software: Possibilities with two vector potential-based formulations. *IEEE Trans. Appl. Supercond.* **2020**, *31*, 5900109. [CrossRef]

93. Benkel, T.; Lao, M.; Liu, Y.; Pardo, E.; Wolfstädter, S.; Reis, T.; Grilli, F. T–A-formulation to model electrical machines with HTS coated conductor coils. *IEEE Trans. Appl. Supercond.* **2020**, *30*, 5205807. [CrossRef]

94. Quéval, L.; Liu, K.; Yang, W.; Zermeño, V.M.; Ma, G. Superconducting magnetic bearings simulation using an H-formulation finite element model. *Supercond. Sci. Technol.* **2018**, *31*, 084001. [CrossRef]

95. Ainslie, M.D.; Quéval, L.; Mataira, R.C.; Bumby, C.W. Modelling the frequency dependence of the open-circuit voltage of a high-T c superconducting dynamo. *IEEE Trans. Appl. Supercond.* **2021**, *31*, 4900407. [CrossRef]

96. Pardo, E.; Šouc, J.; Frolek, L. Electromagnetic modelling of superconductors with a smooth current–voltage relation: Variational principle and coils from a few turns to large magnets. *Supercond. Sci. Technol.* **2015**, *28*, 044003. [CrossRef]

97. Pardo, E.; Kapolka, M. 3D computation of non-linear eddy currents: Variational method and superconducting cubic bulk. *J. Comput. Phys.* **2017**, *344*, 339–363. [CrossRef]

98. Brambilla, R.; Grilli, F.; Martini, L.; Sirois, F. Integral equations for the current density in thin conductors and their solution by the finite-element method. *Supercond. Sci. Technol.* **2008**, *21*, 105008. [CrossRef]

99. Grilli, F.; Brambilla, R.; Martini, L.F.; Sirois, F.; Nguyen, D.N.; Ashworth, S.P. Current density distribution in multiple YBCO coated conductors by coupled integral equations. *IEEE Trans. Appl. Supercond.* **2009**, *19*, 2859–2862. [CrossRef]
100. Brambilla, R.; Grilli, F.; Nguyen, D.N.; Martini, L.; Sirois, F. AC losses in thin superconductors: The integral equation method applied to stacks and windings. *Supercond. Sci. Technol.* **2009**, *22*, 075018. [CrossRef]
101. Morandi, A.; Fabbri, M.; Ribani, P.L.; Dennis, A.; Durrell, J.; Shi, Y.; Cardwell, D. The measurement and modeling of the levitation force between single-grain YBCO bulk superconductors and permanent magnets. *IEEE Trans. Appl. Supercond.* **2018**, *28*, 3601310. [CrossRef]
102. Fabbri, M.; Forzan, M.; Lupi, S.; Morandi, A.; Ribani, P.L. Experimental and numerical analysis of DC induction heating of aluminum billets. *IEEE Trans. Magn.* **2009**, *45*, 192–200. [CrossRef]
103. Perini, E.; Giunchi, G.; Geri, M.; Morandi, A. Experimental and Numerical Investigation of the Levitation Force Between Bulk Permanent Magnet and MgB$_2$ Disk. *IEEE Trans. Appl. Supercond.* **2009**, *19*, 2124–2128. [CrossRef]
104. Prigozhin, L.; Sokolovsky, V. Fast solution of the superconducting dynamo benchmark problem. *Supercond. Sci. Technol.* **2021**, *34*, 065006. [CrossRef]
105. Prigozhin, L.; Sokolovsky, V. Two-dimensional model of a high-T c superconducting dynamo. *IEEE Trans. Appl. Supercond.* **2021**, *31*, 5201107. [CrossRef]
106. Sokolovsky, V.; Prigozhin, L.; Kozyrev, A.B. Chebyshev spectral method for superconductivity problems. *Supercond. Sci. Technol.* **2020**, *33*, 085008. [CrossRef]
107. Ainslie, M.; Grilli, F.; Quéval, L.; Pardo, E.; Perez-Mendez, F.; Mataira, R.; Morandi, A.; Ghabeli, A.; Bumby, C.; Brambilla, R. A new benchmark problem for electromagnetic modelling of superconductors: The high-T c superconducting dynamo. *Supercond. Sci. Technol.* **2020**, *33*, 105009. [CrossRef]
108. Zhang, H.; Machura, P.; Kails, K.; Chen, H.; Mueller, M. Dynamic loss and magnetization loss of HTS coated conductors, stacks, and coils for high-speed synchronous machines. *Supercond. Sci. Technol.* **2020**, *33*, 084008. [CrossRef]
109. Ghabeli, A.; Pardo, E.; Kapolka, M. 3D modeling of a superconducting dynamo-type flux pump. *Sci. Rep.* **2021**, *11*, 10296. [CrossRef]
110. Ghabeli, A.; Ainslie, M.; Pardo, E.; Quéval, L.; Mataira, R. Modeling the charging process of a coil by an HTS dynamo-type flux pump. *Supercond. Sci. Technol.* **2021**, *34*, 084002. [CrossRef]
111. Geng, J.; Matsuda, K.; Fu, L.; Shen, B.; Zhang, X.; Coombs, T. Operational research on a high-Tc rectifier-type superconducting flux pump. *Supercond. Sci. Technol.* **2016**, *29*, 035015. [CrossRef]
112. Geng, J.; Coombs, T. Mechanism of a high-Tc superconducting flux pump: Using alternating magnetic field to trigger flux flow. *Appl. Phys. Lett.* **2015**, *107*, 142601. [CrossRef]
113. Geng, J.; Painter, T.; Long, P.; Gawith, J.; Yang, J.; Ma, J.; Dong, Q.; Shen, B.; Li, C.; Coombs, T. A kilo-ampere level HTS flux pump. *Supercond. Sci. Technol.* **2019**, *32*, 074004. [CrossRef]
114. Zhang, H.; Geng, J.; Coombs, T. Magnetizing high-Tc superconducting coated conductor stacks using a transformer–rectifier flux pumping method. *Supercond. Sci. Technol.* **2018**, *31*, 105007. [CrossRef]
115. Zhou, P.; Ma, G.; Deng, Y.; Nie, X.; Zhai, Y.; Liu, K.; Zhang, H.; Li, Y. A contactless self-regulating HTS flux pump. *IEEE Trans. Appl. Supercond.* **2020**, *30*, 3603006. [CrossRef]
116. Geng, J.; Bumby, C.W.; Badcock, R.A. Maximising the current output from a self-switching kA-class rectifier flux pump. *Supercond. Sci. Technol.* **2020**, *33*, 045005. [CrossRef]
117. Zhai, Y.; Zhou, P.; Li, J.; Sun, C.; Li, Y.; Xiao, L.; Deng, Y.; Ma, G. Performance Investigation of Contactless Self-Regulating HTS Flux Pump. *IEEE Trans. Appl. Supercond.* **2021**, *31*, 4603105. [CrossRef]
118. Li, C.; Geng, J.; Shen, B.; Ma, J.; Gawith, J.; Coombs, T.A. Investigation on the transformer-rectifier flux pump for high field magnets. *IEEE Trans. Appl. Supercond.* **2019**, *29*, 4301105. [CrossRef]
119. Jiang, Z.; Hamilton, K.; Amemiya, N.; Badcock, R.; Bumby, C. Dynamic resistance of a high-Tc superconducting flux pump. *Appl. Phys. Lett.* **2014**, *105*, 112601. [CrossRef]
120. Zhang, H.; Hao, C.; Xin, Y.; Mueller, M. Demarcation currents and corner field for dynamic resistance of HTS-coated conductors. *IEEE Trans. Appl. Supercond.* **2020**, *30*, 6601305. [CrossRef]
121. Oomen, M.; Rieger, J.; Leghissa, M.; ten Haken, B.; ten Kate, H.H. Dynamic resistance in a slab-like superconductor with Jc (B) dependence. *Supercond. Sci. Technol.* **1999**, *12*, 382. [CrossRef]
122. Geng, J.; Coombs, T. An HTS flux pump operated by directly driving a superconductor into flux flow region in the E–J curve. *Supercond. Sci. Technol.* **2016**, *29*, 095004. [CrossRef]
123. Geng, J.; Coombs, T.A. Modeling methodology for a HTS flux pump using a 2D H-formulation. *Supercond. Sci. Technol.* **2018**, *31*, 125015. [CrossRef]
124. Li, C.; Yang, J.; Shen, B.; Ma, J.; Gawith, J.; Öztürk, Y.; Geng, J.; Coombs, T.A. A HTS flux pump simulation methodology based on the electrical circuit. *IEEE Trans. Appl. Supercond.* **2020**, *30*, 4702905. [CrossRef]
125. Bai, Z.; Ding, S.; Li, C.; Li, C.; Yan, G. A newly developed pulse-type microampere magnetic flux pump. *IEEE Trans. Appl. Supercond.* **2010**, *20*, 1667–1670.
126. Bai, Z.; Yan, G.; Wu, C.; Ding, S.; Chen, C. A novel high temperature superconducting magnetic flux pump for MRI magnets. *Cryogenics* **2010**, *50*, 688–692. [CrossRef]

127. Bai, Z.; Chen, C.; Wu, Y.; Zhen, Z. Effect of various pulse wave forms for pulse-type magnetic flux pump. *Cryogenics* **2011**, *51*, 530–533. [CrossRef]

128. Bai, Z.; Ma, C.; Chen, C.; Pang, Y. Study on the excitation of a Bi-2223 small superconducting coil by a pulse-type magnetic flux pump. *IEEE Trans. Appl. Supercond.* **2017**, *27*, 4801705. [CrossRef]

129. Bai, Z.; Cui, X.; Ma, C. Characteristics of Pumping Current in a YBCO Coil by a Pulse-Type Magnetic Flux Pump. *IEEE Trans. Appl. Supercond.* **2021**, *31*, 4602806. [CrossRef]

130. Wang, W.; Lei, Y.; Huang, S.; Wang, P.; Huang, Z.; Zhou, Q. Charging 2G HTS double pancake coils with a wireless superconducting DC p ower supply for persistent current operation. *IEEE Trans. Appl. Supercond.* **2018**, *28*, 0600804. [CrossRef]

131. Zhang, Y.; Wang, W.; Ye, H.; Wang, X.; Gao, Y.; Zhou, Q.; Liu, X.; Lei, Y. Compact linear-motor type flux pumps with different wavelengths for high-temperature superconducting magnets. *IEEE Trans. Appl. Supercond.* **2020**, *30*, 5000305. [CrossRef]

132. Ye, H.; Wang, W.; Zhang, Y.; Wang, X.; Gao, Y.; Zhou, Q.; Liu, X.; Lei, Y. Measuring the output voltage of a linear-motor type flux pump with an insulated HTS coil. *IEEE Trans. Appl. Supercond.* **2020**, *30*, 3800105. [CrossRef]

133. Ye, H.; Wang, W.; Zhang, Y.; Li, H.; Wei, J.; Xu, H.; Zhou, Q.; Liu, X.; Lei, Y. A Linear-Motor Type HTS Flux Pump With Pumped Current Exceeding 640 A. *IEEE Trans. Appl. Supercond.* **2021**, *31*, 3800705. [CrossRef]

134. Zhang, H.; Yang, T.; Li, W.; Xin, Y.; Li, C.; Iacchetti, M.F.; Smith, A.C.; Mueller, M. Origin of the anomalous electromechanical interaction between a moving magnetic dipole and a closed superconducting loop. *Supercond. Sci. Technol.* **2022**, *35*, 045009. [CrossRef]

135. Gawith, J.; Geng, J.; Li, C.; Shen, B.; Zhang, X.; Ma, J.; Coombs, T. A half-bridge HTS transformer–rectifier flux pump with two AC field-controlled switches. *Supercond. Sci. Technol.* **2018**, *31*, 085002. [CrossRef]

136. Leuw, B.; Geng, J.; Rice, J.H.; Moseley, D.A.; Badcock, R.A. A half-wave superconducting transformer-rectifier flux pump using J c (B) switches. *Supercond. Sci. Technol.* **2022**, *35*, 035009. [CrossRef]

137. Sung, H.-J.; Go, B.-S.; Jiang, Z.; Park, M.; Yu, I.-K. Heat loss analysis-based design of a 12 MW wind power generator module having an HTS flux pump exciter. *Phys. C Supercond. Appl.* **2016**, *530*, 133–137. [CrossRef]

138. Sung, H.-J.; Go, B.-S.; Park, H.; Badcock, R.A.; Park, M.; Yu, I.-K. Design, fabrication, and analysis of HTS coils for a 10-kW wind power generator employing a brushless exciter. *IEEE Trans. Appl. Supercond.* **2017**, *27*, 5202305. [CrossRef]

139. Tuvdensuren, O.; Sung, H.; Go, B.; Le, T.; Park, M.; Yu, I. Structural design and heat load analysis of a flux pump-based HTS module coil for a large-scale wind power generator. *J. Phys. Conf. Ser.* **2018**, *1054*, 012084. [CrossRef]

140. Kalsi, S.; Badcock, R.; Hamilton, K.; Storey, J. Homopolar superconducting AC machines, with HTS dynamo driven field coils, for aerospace applications. *IOP Conf. Ser. Mater. Sci. Eng.* **2020**, *756*, 012028. [CrossRef]

141. Kim, J.H.; Quach, H.L.; Boo, C.-J.; Yoon, Y.S.; Jeon, H.; Han, S.; Ko, T.K.; Kim, H.-W.; Jo, Y.-S.; Park, H.J. Fabrication and charging test of HTS field windings using HTS contactless rotary excitation device. *IEEE Trans. Appl. Supercond.* **2019**, *29*, 5203207. [CrossRef]

142. Kim, J.H.; Hyeon, C.J.; Quach, H.L.; Chae, S.H.; Chae, Y.S.; Moon, J.H.; Boo, C.-J.; Yoon, Y.S.; Lee, J.; Jeon, H. Design, analysis, and fabrication of salient field-pole for a 1-kW-class HTS rotating machine. *Cryogenics* **2019**, *97*, 126–132. [CrossRef]

143. Kim, J.H.; Chae, Y.S.; Quach, H.L.; Yoon, Y.S.; Jeon, H.; Han, S.; Ko, T.K.; Lee, J.; Kim, H.-W.; Jo, Y.-S. Fabrication and performance testing of a 1-kW-class high-temperature superconducting generator with a high-temperature superconducting contactless field exciter. *Supercond. Sci. Technol.* **2020**, *33*, 095003. [CrossRef]

144. Parkinson, B.J.; Slade, R.; Mallett, M.J.; Chamritski, V. Development of a cryogen free 1.5 T YBCO HTS magnet for MRI. *IEEE Trans. Appl. Supercond.* **2012**, *23*, 4400405. [CrossRef]

145. Terao, Y.; Ozaki, O.; Ichihara, C.; Kawashima, S.; Hase, T.; Kitaguchi, H.; Kobayashi, S.-i.; Sato, K.-i.; Nakajima, I.; Oonishi, N. Newly designed 3 T MRI magnet wound with Bi-2223 tape conductors. *IEEE Trans. Appl. Supercond.* **2013**, *23*, 4400904. [CrossRef]

146. Parkinson, B.; Bouloukakis, K.; Slade, R. A compact 3 T all HTS cryogen-free MRI system. *Supercond. Sci. Technol.* **2017**, *30*, 125009. [CrossRef]

147. Yokoyama, S.; Miura, H.; Matsuda, T.; Inoue, T.; Morita, Y.; Eguchi, R.; Otake, S.; Tanabe, H.; Sato, S.; Kiss, T. Design and cooling properties of high stable field REBCO superconducting magnet for MRI. *IEEE Trans. Appl. Supercond.* **2020**, *30*, 4400904. [CrossRef]

148. Wang, X.; Wang, W.; Lei, Y.; Gao, Y.; Huang, S.; Liu, X.; Zhou, Q. Electromagnetic design of 1.5 T no-insulation REBCO coil system charged by multiflux pumps for dedicated MRI. *IEEE Trans. Appl. Supercond.* **2019**, *29*, 4601805. [CrossRef]

149. Öztürk, Y.; Shen, B.; Williams, R.; Gawith, J.; Yang, J.; Ma, J.; Carpenter, A.; Coombs, T. Current status in building a compact and mobile HTS MRI instrument. *IEEE Trans. Appl. Supercond.* **2021**, *31*, 4400405. [CrossRef]

150. Baig, T.; Yao, Z.; Doll, D.; Tomsic, M.; Martens, M. Conduction cooled magnet design for 1.5 T, 3.0 T and 7.0 T MRI systems. *Supercond. Sci. Technol.* **2014**, *27*, 125012. [CrossRef]

151. Cosmus, T.C.; Parizh, M. Advances in whole-body MRI magnets. *IEEE Trans. Appl. Supercond.* **2010**, *21*, 2104–2109. [CrossRef]

152. Hahn, S.; Kim, K.; Kim, K.; Hu, X.; Painter, T.; Dixon, I.; Kim, S.; Bhattarai, K.R.; Noguchi, S.; Jaroszynski, J. 45.5-tesla direct-current magnetic field generated with a high-temperature superconducting magnet. *Nature* **2019**, *570*, 496–499. [CrossRef]

153. Miller, J.R. The NHMFL 45-T hybrid magnet system: Past, present, and future. *IEEE Trans. Appl. Supercond.* **2003**, *13*, 1385–1390. [CrossRef]

154. Hamilton, K.; Mataira, R.; Geng, J.; Bumby, C.; Carnegie, D.; Badcock, R. Practical estimation of HTS dynamo losses. *IEEE Trans. Appl. Supercond.* **2020**, *30*, 4703105. [CrossRef]

155. Zhang, H.; Yao, M.; Jiang, Z.; Xin, Y.; Li, Q. Dependence of dynamic loss on critical current and n-value of HTS coated conductors. *IEEE Trans. Appl. Supercond.* **2019**, *29*, 8201907. [CrossRef]

156. Zhang, H.; Wen, Z.; Grilli, F.; Gyftakis, K.; Mueller, M. Alternating current loss of superconductors applied to superconducting electrical machines. *Energies* **2021**, *14*, 2234. [CrossRef]

157. Grilli, F.; Pardo, E.; Stenvall, A.; Nguyen, D.N.; Yuan, W.; Gömöry, F. Computation of losses in HTS under the action of varying magnetic fields and currents. *IEEE Trans. Appl. Supercond.* **2013**, *24*, 78–110. [CrossRef]

158. Morandi, A.; Russo, G.; Fabbri, M.; Soldati, L. Energy balance, efficiency and operational limits of the dynamo type flux pump. *Supercond. Sci. Technol.* **2022**, *35*, 065011. [CrossRef]

159. Walsh, R.M.; Slade, R.; Pooke, D.; Hoffmann, C. Characterization of current stability in an HTS NMR system energized by an HTS flux pump. *IEEE Trans. Appl. Supercond.* **2013**, *24*, 4600805. [CrossRef]

160. Jeon, H.; Lee, J.; Han, S.; Kim, J.H.; Hyeon, C.J.; Kim, H.M.; Kang, H.; Ko, T.K.; Yoon, Y.S. PID control of an electromagnet-based rotary HTS flux pump for maintaining constant field in HTS synchronous motors. *IEEE Trans. Appl. Supercond.* **2018**, *28*, 5207605. [CrossRef]

161. Geng, J.; Wang, B.; Baghdadi, M.; Li, J.; Shen, B.; Zhang, H.; Li, C.; Zhang, X.; Coombs, T.A. Feedback control of a rectifier type HTS flux pump: Stabilizing load current with minimized losses. *IEEE Trans. Appl. Supercond.* **2017**, *27*, 0500104. [CrossRef]